

Generalized Parton Distributions from Hadronic Observables: Zero Skewness

Saeed Ahmad,^{1,*} Heli Honkanen,^{1,†} Simonetta Liuti,^{1,‡} and Swadhin K. Taneja^{1,§}

¹*University of Virginia, 382 McCormick Road,
Charlottesville, Virginia 22904, USA.*

Abstract

We propose a physically motivated parametrization for the unpolarized generalized parton distributions. At zero value of the skewness variable, ζ , the parametrization is constrained by simultaneously fitting the experimental data on both the nucleon elastic form factors and the deep inelastic structure functions. A rich phenomenology can be addressed based on this parametrization. In particular, we track the behavior of the average: *i*) interparton distances as a function of the momentum fraction, X , *ii*) X as a function of the four-momentum transfer, t ; *iii*) the intrinsic transverse momentum k_{\perp} as a function of X . We discuss the extension of our parametrization to $\zeta \neq 0$ where additional constraints are provided by higher moments of the generalized parton distributions obtained from *ab initio* lattice QCD calculations.

PACS numbers: 13.60.Hb, 13.40.Gp, 24.85.+p

arXiv:hep-ph/0611046v2 31 Aug 2007

*E-mail: sa8y@virginia.edu

†E-mail: hh9e@virginia.edu

‡E-mail: sl4y@virginia.edu

§E-mail: taneja@cpht.polytechnique.fr; Present address: Ecole Polytechnique, CPHT, F91128 Palaiseau Cedex, France

I. INTRODUCTION

Most information on the quark and gluon structure of hadrons has come so far from inclusive Deep Inelastic Scattering (DIS) type experiments. With an appropriate selection of probes and reactions, accurate measurements conducted through the years allowed one to map out in detail the different components of proton structure, the Parton Distribution Functions (PDFs) in a wide kinematical region of the four-momentum transfer, Q^2 , and of the longitudinal momentum fraction of the proton's momentum, $x_{Bj} = Q^2/2M\nu$, ν being the energy transfer and M the proton mass.

Recently, a whole new dimension was added to our understanding of hadronic structure, with the observation that in a number of exclusive experiments one can, on one side, study a wider range of flavor and spin dependent combinations of PDFs with respect to those obtained from inclusive scattering, and on the other, new, qualitatively different information can in principle be extracted from a specific class of experiments, including Deeply Virtual Compton Scattering (DVCS), and hard Exclusive Meson Production (EMP). The information from these processes is coded in terms of “off-forward” contributions, or the Generalized Parton Distributions (GPDs) [1, 2, 3]. GPDs allow us to access partonic configurations with a given longitudinal momentum fraction, similarly to DIS, but also at a specific (transverse) location inside the hadron [4].

PDFs are extracted directly from inclusive measurements of the DIS structure functions at a given Q^2 . Perturbative QCD (PQCD) evolution connects the PDF values at Q^2 with the ones at an initial scale, Q_o^2 . The initial PDFs are usually given in parametric forms that broadly reproduce the behavior expected in a few limiting cases: they include, for instance, a Regge-type behavior at low x_{Bj} , and a quark-counting type behavior in the limit $x_{Bj} \rightarrow 1$. A number of sum rules such as Adler's, and the momentum sum rule provide additional constraints. It is also generally understood that the proton is an “emptier” object dominated by its minimal – valence – components at low Q^2 . The sea quark content is determined both by quark-antiquark pairs and gluons radiations which characterize perturbative evolution from the initial low scale, and by “intrinsic” components also expected to be present at low scales. PDF parametrizations have become more sophisticated through the years both because of the continuous addition of DIS data in increasingly extended kinematical regimes, and because of phenomenological developments allowing one to extend the number of hard processes from which PDFs can be extracted. It is now possible to describe the proton structure functions with relative accuracy in the regime: $10^{-4} \lesssim x_{Bj} \lesssim 0.75$, and $1 \lesssim Q^2 \lesssim 10^4 \text{ GeV}^2$ [5].

The matching between measured quantities and leading order predictions for DVCS/EMP and GPDs should proceed, in principle, similarly to the inclusive case, in view of the factor-

ization theorem discussed in Ref. [2]. There are however a few important caveats due to the fact that GPDs describe the non-perturbative contribution to an *amplitude*. Both the real and imaginary parts of the amplitude are physical observables in the $\gamma^*P \rightarrow \gamma P'$ process, obtained from the interference term for the DVCS and Bethe-Heitler (BH) processes (see [6] and reviews in [7, 8]).

The leading order amplitude for DVCS is shown in Fig. 1 along with the relevant kinematical variables, namely: the longitudinal momentum fraction taken by the initial quark, X , $Q^2 \equiv -q_\mu^2$, the four-momentum transfer squared between the initial and final proton states, $t \equiv -\Delta^2$, and the longitudinal momentum transfer fraction of the initial proton momentum, the so-called “skewness”, ζ . Because of the extra two parameters, ζ and t , obtaining initial parametrizations in a similar fashion as for inclusive parton distributions is a formidable task. Furthermore, experimental measurements of GPDs are remarkably more complicated than in inclusive DIS, essentially due to the exclusive nature of DVCS/EMP. Despite the high performance of current facilities such as Jefferson Laboratory, one cannot realistically expect in the near future a similar amount and quality of data as in inclusive experiments.

Given the importance of the physics underlying GPDs, and the far reaching consequences of their study related to a number of key questions such as the contributions of the partons angular momentum to the nucleon’s spin, the exploration of 3D spatial images of the nucleon, and the connection to Transverse Momentum Distributions (TMDs) [7, 8], it is most important at the present stage, to explore whether currently available inclusive data can also provide additional constraints on GPDs. These constraints can both supplement the, so far, scarce experimental results obtained directly from DVCS/EMP, and at the same time provide a guidance for future precision exclusive experiments at both Jefferson Lab at 12 GeV, and future colliders.

Experimental constraints from other-than-DVCS-type data on GPDs are obtained from: *i*) The nucleon form factors providing integrals of GPDs over X at a fixed t ; *ii*) The PDFs, representing the $(\zeta, t \rightarrow 0)$ limit of GPDs. An additional check is also provided by the relation, through simple Fourier transformation, between zero skewedness GPDs and Impact Parameter Dependent PDFs (IPPDFs) [4]. Physically meaningful GPDs should in fact reproduce the correct behavior of partonic configuration radii obtained from their impact parameter space representation.

Because both the form factors and PDFs are independent of ζ , these constraints apply exclusively to the case $\zeta = 0$, $t \equiv -\Delta_\perp^2$. Zero skewedness GPDs extracted using available experimental constraints were first considered in the initial phenomenological studies of Refs. [9, 10, 11, 12]. Fully quantitative fits were subsequently performed in Refs. [13, 14]. Defining a parametrization at $\zeta \neq 0$, however, requires the additional condition of polynomiality to be satisfied [7] Moreover, a physical interpretation in terms of partonic components

becomes less transparent both at $X = \zeta$ – the “stopped returning quark” region – and at $X < \zeta$ where the dominating process is scattering from a $q\bar{q}$ pair emerging from the initial nucleon. The only guidance for a parametrization at $\zeta \neq 0$ has been provided, so far, by the Double Distribution (DD) hypothesis [15, 16], that has a built-in property of polynomiality. More recently, the Mellin-Barnes integral representation [17], and the dual representation [18] were proposed, where the GPDs were obtained within a generalization of the anti-Mellin transform approach used for PDFs. Nevertheless, similarly to what found for DIS [19, 20], the extraction of GPDs from moments formally requires a continuation to complex n that, because of an oscillating term inherent in the moments integral, can be a source of ambiguities. This has so far hampered an accurate extraction using other than simplified models.

Motivated by this situation, in this paper, we introduce a practical method to extract GPDs from experimental data, that can be extended also at $\zeta \neq 0$, by using additional ζ -dependent constraints from *ab-initio* lattice QCD calculations of the first three moments of GPDs [21, 22]. We stress that differently from the DDs, representing a model calculation, our approach is, for the first time to our knowledge, an attempt to obtain a realistic parametrization. Given the paucity of current direct experimental measurements of GPDs, our goal is to provide more stringent, model independent predictions that will be useful both for model builders, in order to understand the dynamics of GPDs, and for the planning of future DVCS type experiments.

Our paper organization is as follows: In Section II we describe our approach for a physically motivated parametrization valid both in the $\zeta = 0$ and $\zeta \neq 0$ cases. We consider the unpolarized GPDs, H and E , for which the lattice moments are the most accurate. In Sections III, and IV we discuss in detail the $\zeta = 0$ case: in III we perform a detailed comparison with the data on both form factors and PDFs; In IV we show the phenomenology of GPDs at $\zeta = 0$ by illustrating the role of the various quantities: the quarks transverse radii $\langle y_q \rangle$, the intrinsic transverse momentum \mathbf{k}_\perp , the average X values contributing to the nucleon form factors as a function of t . We also discuss the feasibility of the extraction using lattice results and introduce our method. For ease of presentation, a number of graphs and more quantitative results on the $\zeta \neq 0$ case are reported in a following paper [23]. In Section V we draw our conclusions.

II. A PHYSICALLY MOTIVATED PARAMETRIZATION FOR UNPOLARIZED GPDS

GPDs parameterize the non-perturbative vertex in the DVCS process depicted in Fig. 1. Scattering from an unpolarized proton (neutron) is described by two independent GPDs:

H , and E , from the vector (γ_μ) and tensor ($\sigma_{\mu\nu}$) interactions, respectively, that depend on three kinematical invariants, besides the initial photon's virtuality, Q^2 : the longitudinal momentum transfer, $\zeta = Q^2/2(Pq)$, the four-momentum transfer squared, $\Delta^2 = -t$, and the variable $X = (kq)/(Pq)$, representing the Light Cone (LC) momentum fraction carried by the struck parton with momentum k . The relations between the variables used in this paper and the analogous set of kinematical variables in the “symmetric” system, frequently used in the literature are given along with the definitions of the hadronic tensors components in Refs. [24]. Note the slightly different choice from Ref. [25] for which the sea quarks GPDs are also defined at $X > 0$ (see Appendix A).

At present, due to both the small experimental coverage mentioned above, and to the somewhat less transparent physical interpretation of the observables, an important role in the shaping of a parametrization for GPDs is played by the intuition on the underlying non-perturbative dynamics.

In the general case of non-zero skewedness, one distinguishes two kinematical regions: *i*) $\zeta < X < 1$, where the dominant process is where a quark from the initial proton with LC momentum fraction X , is struck by the initial photon and is subsequently reabsorbed in the proton (with $X - \zeta > 0$); *ii*) $0 < X < \zeta$, where the final quark propagates backwards, or, correspondingly, a quark-antiquark pair from the initial proton, with an asymmetric partition of LC momenta, participates in the scattering process.

The physics of the two regions is most easily understood within a field theoretical description where the lowest order is given by a covariant quark-nucleon scattering amplitude, with the nucleon-quark-diquark vertex being a Dirac matrix multiplied by a scalar function.¹ Physical intuition on DVCS processes can then be obtained by viewing the covariant diagrams as the sum of all possible time ordered diagrams. The invariant amplitude for DVCS corresponds to $4!$ time ordered diagrams. They are grouped into the following classes of processes (Fig. 2): **(a)** all particles moving forward (Fig. 2a); **(b)** the initial photon splits into a quark-antiquark pair that then interacts with the hadronic system; **(c)** an initial quark-antiquark pair originates from the initial proton and scatters from the probe (Fig. 2b). Each process has a corresponding “crossed term” (not drawn in the figure).

¹ The most general case involves a linear combination of Dirac matrices [26, 27])

We consider the following choice of frame, and four-momentum components:²

$$q \equiv (0; \mathbf{q}, 0) \quad (1a)$$

$$P \equiv \left(P + \frac{M^2}{2P}; \mathbf{0}, P \right) \quad (1b)$$

$$k \equiv \left(XP + \frac{\mathbf{k}_\perp^2 + m_q^2}{2XP}; \mathbf{k}_\perp, XP \right) \quad (1c)$$

$$k_X \equiv \left((1-X)P + \frac{\mathbf{k}_\perp^2 + M_X^2}{2(1-X)P}; -\mathbf{k}_\perp, (1-X)P \right) \quad (1d)$$

$$k' \equiv \left((X-\zeta)P + \frac{(\mathbf{k}_\perp - \Delta_\perp)^2 + m_q^2}{2(X-\zeta)P}; \mathbf{k}_\perp - \Delta_\perp, (X-\zeta)P \right) \quad (1e)$$

$$P' \equiv \left((1-\zeta)P + \frac{\Delta_\perp^2 + M^2}{2(1-\zeta)P}; -\Delta_\perp, (1-\zeta)P \right) \quad (1f)$$

$$\Delta \equiv \left(\zeta P + \frac{-t + \Delta_\perp^2}{2\zeta P}; \Delta_\perp, \zeta P \right) \quad (1g)$$

where, moreover, $q' = q + \Delta$. Eq. (1d) gives the components of a spectator system, *i.e.* a *diquark*, that is our main assumption in the following sections, namely that the spectral distribution of states appearing in principle in the quark correlator can be replaced by one state with a given mass. Finally, in the given frame, contributions dominated by the hadronic components of the initial photon (case **(c)**) are absent. More generally, all processes where one of the particles is moving backwards (or one of the particles has a longitudinal momentum opposite to the protons' one) vanish as inverse powers of P .

A. The $X > \zeta$ region

At $X > \zeta$, the proton splits into a quark carrying a LC momentum fraction $X = k^+/P^+$, transverse momentum \mathbf{k}_\perp , and a spectator system with $1-X = k_X^+/P^+$, and $-\mathbf{k}_\perp$ (Fig. 2a). Similarly the right side vertex describes the coalescence of the final quark and the spectator system into an outgoing proton (all particles are moving forward). With an appropriate choice for the $P \rightarrow (k k_X)$ and $P' \rightarrow (k' k_X)$ vertices, *i.e.* assuming a spectator diquark with both scalar and axial vector components, the DVCS matrix element, $F(X, \zeta, t)$, can be

² We use the notation $a^\mu \equiv (a^0 \equiv E_a; \mathbf{a}_\perp, a^3)$, and $a^\pm = (a^0 \pm a^3)/\sqrt{2}$.

written at leading order in Q^2 , as (see also Ref. [28]):

$$\begin{aligned}
F(X, \zeta, t) &= \frac{1}{2P^+} \left[\bar{U}(P', S') \left(\gamma^+ H^q(X, \zeta, t) + \frac{i\sigma^{+\mu}\Delta_\mu}{2M} E^q(X, \zeta, t) \right) U(P, S) \right] \\
&= \sqrt{1-\zeta} H^q(X, \zeta, t) - \frac{1}{4} \frac{\zeta^2}{\sqrt{1-\zeta}} E^q(X, \zeta, t) \\
&= \frac{\sqrt{X}\sqrt{X-\zeta}}{1-X} \int d^2\mathbf{k}_\perp \rho^q(k^2, k'^2).
\end{aligned} \tag{2}$$

In Eq. (2):

$$\sqrt{1-\zeta} = \frac{1}{2P} \text{Tr}\{U(P, S)\bar{U}(P', S')\gamma^+\} \tag{3a}$$

$$\frac{1}{4} \frac{\zeta^2}{\sqrt{1-\zeta}} = \frac{1}{2P} \text{Tr}\{U(P, S)\bar{U}(P', S')\frac{i}{2M}\sigma^{+\mu}\Delta_\mu\}, \tag{3b}$$

where the traces over the nucleon spinors are for the *same spin*, $S = S'$, case. The factors $\sqrt{X}\sqrt{X-\zeta}$, are obtained similarly from the traces over the quarks spinors implicit in Eq. (2) [28]. Having taken care of the spin structure, we then model $\rho^q(k^2, k'^2)$ as:

$$\rho^q(k^2, k'^2) = \mathcal{N} \frac{\phi(k'^2)}{k'^2 - m_q^2} \frac{\phi(k^2)}{k^2 - m_q^2}, \tag{4}$$

m_q is the struck quark's mass, $\phi(k^2)$ is a scalar vertex function whose form will be specified in Section III, and \mathcal{N} is a normalization constant.

By using the components in Eqs. (1a) we obtain for $H^q(X, \zeta, t)$:

$$\begin{aligned}
H^q(X, \zeta, t) &= \int \frac{d^2\mathbf{k}_\perp}{(1-X)} \frac{\mathcal{A} \phi(k^2, \lambda) \phi^*(k'^2, \lambda)}{[(2E_k)(E_p - E_k - E_X)] [(2E_{k'})(E_{p'} - E_{k'} - E_X)]} \\
&= \int d^2\mathbf{k}_\perp \frac{\mathcal{A} \phi(k^2, \lambda) \phi^*(k'^2, \lambda)}{\left(\mathcal{M}_0^2(X) - \frac{\mathbf{k}_\perp^2}{1-X} - m_q^2 \right) \left(\mathcal{M}_\zeta^2(X) - \frac{1-\zeta}{1-X} \left[\mathbf{k}_\perp - \frac{1-X}{1-\zeta} \Delta \right]^2 - m_q^2 \right)},
\end{aligned} \tag{5}$$

where we have rendered explicit the connection between the time ordered diagram in Fig. 2a and the covariant expression in Eq. (4). Furthermore, in Eq. (5):

$$\mathcal{M}_\zeta^2(X) = (X - \zeta)/(1 - \zeta)M^2 - (X - \zeta)/(1 - X)M_X^{q2}, \tag{6}$$

and

$$\mathcal{A} = \mathcal{N} \frac{X}{1-X} \sqrt{\frac{X-\zeta}{X}} \frac{1}{\sqrt{1-\zeta}} \tag{7}$$

The GPD, $E^q(X, \zeta, t)$ is modeled similarly to H^q , but imposing a different normalization, namely: $\mathcal{N}_E = \kappa_q \mathcal{N}_H$, ($\mathcal{N}_H \equiv \mathcal{N}$ in Eq. (4)), where κ_q is the quark's q component of the anomalous magnetic moment.

The invariant mass of the spectator, $k_X^2 \equiv M_X^q$, appearing in Eq. (5) through Eq. (6), is a flavor dependent parameter. Both in Eq. (5), and in the results presented in Section III the value of M_X^q is considered to be fixed for each configuration. However, a spectral distribution in $M_X^{q2} \equiv (P - k)^2$ should in principle be introduced for large values of the invariant mass. This affects mainly the low X region, *i.e.* where M_X^q is large, and it has been successfully reproduced in deep inelastic scattering processes by introducing an M_X^q dependence of the spectral function consistent with Regge behavior [29]. The role of t -channel exchanges in DVCS and related processes was addressed recently in [30] where the rather extreme point of view was taken that GPDs measure mostly the parton content of the reggeons. A full treatment of this important point is beyond the scope of the present work and will be considered in a forthcoming paper. Here, we introduce directly a ζ and t dependent Regge motivated term, in addition to the “diquark” term given by Eq. (5), and we study their relative contribution to phenomenology in Section IV.

In Eq. (5) we have written explicitly the dependence on the size parameter λ , which is similar to the one used in the “overlap representation” based models (cf. *e.g.* the equivalent parameter for the more commonly used “gaussian form” discussed in Ref. [31]). We underline that the model considered here is, in fact, consistent with the “overlap representation” derived for DVCS in [25, 32], but, due to the covariance of the vertex function, it differs from constituent quark models. Due to the covariance of the vertex function, the spectator model captures two essential features, or “self-consistency” conditions: *i)* the GPDs are not imposed to be zero at the endpoint $X = \zeta$, thus allowing for an imaginary part of the DVCS amplitude. This is also in accordance with the experimental observation from DVCS experiments at both HERMES [33] and Jefferson Laboratory [34]; *ii)* the GPDs are continuous at the endpoint $X = \zeta$. Calculations similar to the one presented here were performed both within QED [25], and in a simplified version of the covariant model with scalar particles in [35]. Both cases are however presented as illustrations that are not meant to be quantitatively compared to data. On the other side, attempts similar to ours to extract GPDs from the data [13], although physically motivated, are leaning towards mathematical forms similar to “PDF-type” parametrizations.

This paper’s goal is to combine both the essential dynamical aspects described above, with a fully quantitative analysis that is made possible by the flexibility of our simplified model. A direct comparison with inclusive experimental data is only possible in the $\zeta = 0$ region. At $\zeta \neq 0$, one needs to include in the analysis the higher moments of GPDs, that are ζ -dependent, besides the nucleon form factors. Higher moments are currently available from lattice QCD [36] and can be implemented within an extension of our analysis to this case.

B. A special case: $\zeta = 0$

The case $\zeta = 0$ where the momentum transfer is entirely transverse, $\Delta^2 \equiv -\Delta_\perp^2$, plays a special role since processes of type **(b)**, and **(c)** (see Fig. 2) are suppressed.

The following relations hold (we set $H^q(X, 0, t) \equiv H^q(X, t)$):

$$H^q(X, t = 0) = q(X), \quad (8)$$

where $q(X)$ is the parton distribution for quark “ q ”. The transverse DIS structure function, $F_T(X) \equiv F_1(X)$ is given by:

$$F_T^p(X) = \frac{4}{9}H^u(X, 0) + \frac{1}{9}H^d(X, 0) + \frac{1}{9}H^s(X, 0) \quad (9a)$$

$$F_T^n(X) = \frac{1}{9}H^u(X, 0) + \frac{4}{9}H^d(X, 0) + \frac{1}{9}H^s(X, 0), \quad (9b)$$

where we implicitly assume the Q^2 dependence, and the structure function F_2 is obtained from Callan-Gross’s relation: $2X F_1(X) = F_2(X)$ Furthermore, the following relations:

$$\int_0^1 dX H^q(X, t) = F_1^q(t) \quad (10a)$$

$$\int_0^1 dX E^q(X, t) = F_2^q(t), \quad (10b)$$

define the connection with the quark q ’s contribution to the Dirac and Pauli form factors. The proton and neutron form factors are obtained as:

$$F_{1(2)}^p(t) = \frac{2}{3}F_{1(2)}^u(t) - \frac{1}{3}F_{1(2)}^d(t) + \frac{1}{3}F_{1(2)}^s(t) \quad (11a)$$

$$F_{1(2)}^n(t) = -\frac{1}{3}F_{1(2)}^u(t) + \frac{2}{3}F_{1(2)}^d(t) + \frac{1}{3}F_{1(2)}^s(t), \quad (11b)$$

where $F_{1(2)}^s(t)$ was found to be consistent with zero [37]. In our analysis we fitted linear combinations of the integrals of GPDs obtained from Eq. 10 to the electric and magnetic form factors, for which the experimental data are more readily accessible:

$$G_E^{p(n)}(t) = F_1^{p(n)}(t) + \frac{t}{4M^2}F_2^{p(n)}(t) \quad (12a)$$

$$G_M^{p(n)}(t) = F_1^{p(n)}(t) + F_2^{p(n)}(t). \quad (12b)$$

Eqs. (8,9,10,11,12) define all the constraints used in our fit. A detailed description of the results of the fit is presented in Section III.

C. The $X < \zeta$ region

When $X < \zeta$, the dominating process is the one where a quark with $X = k^+/P^+$, and transverse momentum, \mathbf{k}_\perp , and an anti-quark with $\zeta - X = k'^+/P^+ > 0$, and $\mathbf{k}'_\perp = \mathbf{\Delta}_\perp - \mathbf{k}_\perp$

emitted from the initial proton, undergo the electromagnetic interaction (Fig. 2b). While in the calculation of form factors, and of the $\zeta = 0$ GPDs, process **(b)** is always suppressed, at $\zeta \neq 0$, it can represent a situation with “all particles moving forward” so long as $X < \zeta$. This is evident by inspecting the energy denominators in this kinematical region that are, in fact, characterized by similar cancellations as for process **(a)** at $X > \zeta$ (Eq. (5)).

The physical interpretation of this region still presents, however, a few debatable points. Within the overlap representation, GPDs are given exclusively by the higher Fock states – a minimum requirement being the $(q\bar{q}qq)$ state. The latter are not sufficiently constrained by phenomenological studies. Recently, higher Fock states were considered in Ref. [38] within a LC constituent quark model for the pion GPDs, where their contribution was shown to be indeed sizable at $X = \zeta$ (the so-called crossover point). Notice, however, that as X decreases, a large number of Fock components would need to be introduced. Quantitative calculations were performed both within QED [25], and in a scalar model [35], where it was shown that the sum of the $X > \zeta$ and $X < \zeta$ contributions naturally provides a covariant expression, thus satisfying the polynomiality condition. This is the independence of the form factor from the parameter ζ , which if not observed, would signal the presence of an artificial frame dependence [32]. An alternative description is where the $q\bar{q}$ pair contribution to GPDs is interpreted as t -channel exchanges [15] (modulo appropriate color factors [32]) of either a single meson, or a tower of mesons, as recently proposed in [18].

Lacking a uniform picture, and given the important role that will be played by GPDs in the $X < \zeta$ region for the interpretation of a number of experiments: from $\bar{p}p$, and $\bar{p}A$, exclusive reactions [39], to deep inelastic pion production and other semi-inclusive experiments at forthcoming facilities, we propose a strategy that can provide further guidance in this region.

Starting from the accurate parametrization of the $\zeta = 0$ case presented in this paper, and obtained directly from experimental data, we subsequently study the constraints for the $\zeta > 0$ case. These are provided, on one side, by the higher order Mellin moments of H and E 's that govern the behavior with ζ of the GPDs. Moments of order $n \leq 3$ can be obtained from lattice calculations [21, 22]. On the other side, we notice that the $X > \zeta$ region is dominated by the same “valence type” configurations as for the $\zeta = 0$ case described by Eq. (5), and it can be therefore obtained by extending our $\zeta = 0$ parametrization to this kinematics using the same constraints. In this approach, polynomiality is imposed at every step, within a “bottom up” type of approach, rather than the “top down” method implicit in both the double distributions [15]. In Section IV we illustrate the type of information that can be obtained from lattice results in the specific cases of $\zeta = 0$. Information on the $X < \zeta$ behavior using higher moments, combined with the experimentally constrained $X > \zeta$ behavior, is extracted according to a deconvolution procedure described in detail in

a forthcoming paper [23].

III. RESULTS

We now present our quantitative determination of the unpolarized GPDs, H and E , obtained at $\zeta = 0$ using all available data on the proton and neutron electromagnetic form factors, as well as the valence quarks distributions from DIS measurements. Our fit is obtained at a low scale, $Q_o^2 \approx 0.1 \text{ GeV}^2$, in line with the approach of Ref. [40] where it is assumed that at a low scale the nucleon consists mostly of valence quarks, the bulk of the gluon and anti-quark distributions being generated dynamically.

We reiterate that, although direct measurements of DVCS cannot be currently implemented, our procedure produces effectively a “parametrization”, in that parameter-dependent physically motivated functional forms are fitted to data. The goodness of the fit is tested by means of a χ^2 , whose values, along with the parameter errors have been quantitatively evaluated and are given below. We, of course, support the future usage of DVCS data because they are more directly linked to GPDs [41], and we are actively considering their implementation [23]. The amount of data and their kinematical range is however too limited at present to provide sensibly more stringent constraints. We would also like to add that parametrization shapes do represent a possible bias in the present analysis as well as in any type of fitting (see *e.g.* discussion in Ref. [42]), for instance the shape of the gluon distribution functions has been oscillating through the years between “valence-like” to hard-peaked at $x \rightarrow 0$. The problem of the initial bias can be attacked in a similar way for GPDs, by tuning in possible new shapes as constraints from new sets of data become available, allowing for more refined fitting.

Starting from Eq. (5), with the inclusion of the Regge term discussed in Section II A we obtained two slightly different forms that are both constrained by current experimental data:

Set I

$$H^I(X, t) = G_{M_X^I}^{\lambda^I}(X, t) X^{-\alpha^I - \beta_1^I(1-X)^{p_1^I} t} \quad (13)$$

$$E^I(X, t) = \kappa G_{M_X^I}^{\lambda^I}(X, t) X^{-\alpha^I - \beta_2^I(1-X)^{p_2^I} t} \quad (14)$$

Set II

$$H^{II}(X, t) = G_{M_X^{II}}^{\lambda^{II}}(X, t) X^{-\alpha^{II} - \beta_1^{II}(1-X)^{p_1^{II}} t} \quad (15)$$

$$E^{II}(X, t) = G_{M_X^{II}}^{\tilde{\lambda}^{II}}(X, t) X^{-\tilde{\alpha}^{II} - \beta_2^{II}(1-X)^{p_2^{II}} t} \quad (16)$$

All parameters except for p_1 and p_2 are flavor dependent; we omit, however, the “q” symbol (unless specifically needed) for ease of presentation. The function G has the same form for both parametrizations, I and II:

$$G_{M_X}^\lambda(X, t) = \mathcal{N} \frac{X}{1-X} \int d^2\mathbf{k}_\perp \frac{\phi(k^2, \lambda)}{D(X, \mathbf{k}_\perp)} \frac{\phi(k'^2, \lambda)}{D(X, \mathbf{k}_\perp + (1-X)\mathbf{\Delta}_\perp)}, \quad (17)$$

where

$$D(X, \mathbf{k}_\perp) \equiv k^2 - m^2, \quad (18)$$

and

$$k^2 = XM^2 - \frac{X}{1-X} M_X^2 - \frac{\mathbf{k}_\perp^2}{1-X} \quad (19)$$

$$k'^2 = XM^2 - \frac{X}{1-X} M_X^2 - \frac{(\mathbf{k}_\perp - (1-X)\mathbf{\Delta}_\perp)^2}{1-X}, \quad (20)$$

m being the struck quark mass, and M , the proton mass. The normalization factor includes the nucleon-quark-diquark coupling, and it is set to $\mathcal{N} = 1 \text{ GeV}^6$. Eq. (17), was obtained using the following Dirac structure for the vertex in Eq. (5):

$$\Gamma(k, P)_{\alpha\beta} = \sum_\lambda u_\alpha(k, \lambda) \bar{U}_\beta(P, \lambda) \phi(k^2, \lambda^2), \quad (21)$$

where [27]³

$$\phi(k^2, \lambda) = \frac{k^2 - m^2}{|k^2 - \lambda^2|^2}. \quad (22)$$

Finally, the u and d quarks contributions to the anomalous magnetic moments are:

$$\kappa \equiv \kappa^q = \begin{cases} \kappa^d = 2.03, & \text{for } q = d \\ \kappa^u/2 = 1.67/2, & \text{for } q = u \end{cases}. \quad (23)$$

A few comments are in order:

i) At present it is important to provide a parametrization that allows one to address a richer phenomenology, including the interplay of coordinate and momentum space observables. The spectator model used here is ideal because despite its simplicity, it has proven to be sufficiently flexible to describe (and predict) the main features of a number of distribution and fragmentation functions in the intermediate and large X regions, as well as the unintegrated PDFs [26, 43]. The spectator system can be a scalar or a spin 1 vector, thus allowing

³ With this choice of diquark form factor, one ensures that the value of the quark mass, or equivalently the position of the pole in the quark propagator, does not play a dynamical role in the model. The values of the quark masses are consequently not determined in our fit.

us to access both the u and d quark distributions. In Ref. [26] it was shown that the value of the spectator mass in the two cases is crucial in shaping the parametrizations for u and d quarks respectively. Here we have let also the mass parameter λ be flavor dependent.

ii) Similarly to the case of DIS structure functions the spectator model is not able to reproduce quantitatively the very small X behavior of the GPDs (this problem is again present in the very small t behavior of the nucleon form factors and GPDs). This mismatch is not very visible in the results of Refs. [26, 27, 43] because of the linear scale used in the plots; it is, however, responsible for a violation of the baryon number sum rule that becomes particularly important in GPD parametrizations since one needs to achieve a precise agreement with the nucleon form factors as well. We introduced therefore a “Regge-type” term multiplying the spectator model function $G_{M_X}^\lambda$ in Eqs. (13,14,15,16). A similar behavior was considered in the “profile functions” of Refs. [13, 14]. However, our procedure is distinctively different (as discussed also in our results below) because in our case a simultaneous fit to both the PDFs from DIS and to the nucleon form factors is performed. In Refs. [13, 14] the PDF limit (Eq. (8)) is trivially satisfied, whereas the form factors and the additional constraints from the expected Regge behavior are subsequently used to define the GPDs shape.

iii) We considered the two variants shown above, in order to estimate the sensitivity to different procedures as also described in *ii*). Set I and II differ in the determination of E , that is in principle unrelated to the forward PDFs, and therefore less constrained by the data.

A. Results of fit from nucleon form factors and PDFs

The experimental data on the nucleon form factors implemented in the fit are: G_E^p [44], G_M^p [45], G_E^n [46], G_M^n [47] and G_E^p/G_M^p [48]. The data selection is the same that was used in Ref. [49], where for $-t > 1 \text{ GeV}^2$ only the measurements based on polarization transfer techniques were considered, while the Rosenbluth separation ones were discarded. In the fitting procedure all of the form factor data enter simultaneously in the parametrizations for H^q and E^q , respectively. This is at variance with implementing data on the F_1 and F_2 form factors, which also require extrapolations from different data sets. By fitting directly to the electric and magnetic form factors we obtained a more precise determination since no data manipulation is necessary. In particular, an accurate description of the low t region is important in view of future comparisons with the lattice determinations [23].

The χ^2 per number of data points in each data set, as well as for the total number of data points, is listed in Table I for parametrization Sets I and II. The comparison with form factor data is shown in Fig. 3 for the proton, and in Fig. 4 for the neutron. The ratio

G_M^p/G_E^p is shown in Fig. 5. To check to what extent our parametrization is dominated by the data from G_M^p , we also repeated the fit by weighting each form factor by the number of corresponding data points. The effect for the listed values of χ^2 was less than 2%.

Data Set	χ^2/N_{data} Set 1	χ^2/N_{data} Set 2	Data Points
G_{E_p}	1.049	0.963	33
G_{M_p}	1.194	1.220	75
G_{E_p}/G_{M_p}	0.689	0.569	20
G_{E_n}	0.808	1.059	25
G_{M_n}	2.068	1.286	24
TOTAL	1.174	1.085	177

TABLE I: The χ^2/N_{data} of the different nucleon form factors obtained from Set I and Set II. N_{data} is the number of data points available for each set of form factor data.

The parameters in the $t \rightarrow 0$ limit were determined by fitting to the LO set of Alekhin PDFs [50] within the range $10^{-5} \leq x \leq 0.8$ and $4 \leq Q^2 \leq 240 \text{ GeV}^2$, and imposing the baryon number and momentum sum rule such that:

$$\int_0^1 dX u(X, Q_0^2) = 2 \quad (24)$$

$$\int_0^1 dX d(X, Q_0^2) = 1 \quad (25)$$

$$\int_0^1 dX X [u(X, Q_0^2) + d(X, Q_0^2)] = 1. \quad (26)$$

The parameters involved in this step, M_X^q , λ^q and α^q , $q = u, d$, obtained at an initial scale Q_o^2 ($Q_o^2 = 0.094 \text{ GeV}^2$), are listed in Table II. Notice that: *i*) they are the same for both Sets I and II; *ii*) in Set I they are by definition the same for the functions H and E (see Eqs. (13,14)). The parameters in the PDCD evolution were chosen as in CTEQ6L1 [51].

Flavor	M_X (GeV)	λ (GeV)	α
u	0.4972	0.9728	1.2261
d	0.7918	0.9214	1.0433

TABLE II: Parameters fixing the shape of H^q , $q = u, d$, at $t = 0$. The parameters are the same for both Set I and Set II. Moreover, they also define the $t = 0$ limit for E^q in Set I, as it can be seen from the definitions given in Eqs. (13,14).

Similar results can be in principle obtained from other current PDF parametrizations [51, 52], however the valence contributions from Ref. [50] tend to more readily agree with the shape given in Eqs. (13,15). The experimental data on DIS structure functions were not

used directly, because our parametrization does not include an ansatz for the sea quarks. Therefore it is not possible to reproduce within this context the low x behavior of the DIS structure function $F_2(X, Q^2)$. For the same reason, the estimated errors of Alekhin's PDFs were not used in the fit. This aspect is beyond the scope of the present analysis, and will be improved in future work on by extending our model to include sea quarks [23]. It should be noticed that, as in similar approaches [26, 27, 35], higher-order effects might be important especially considering the low value of the initial scale, Q_0^2 , resulting from the requirement that only valence quarks contribute to the momentum sum rule (Eq. (26)). However, on one side some of the previous evaluations [27, 40] do not seem to find quantitatively large higher order effects, on the other, the fact that Q_0^2 is a parameter in our model, determined itself by fitting the valence PDF to the (parametrization of the) data [50] in the large Q^2 regime, lends self-consistency to our procedure (see also [40, 53]). In order to gauge the effects of perturbative evolution, a dedicated study of NLO is being considered in upcoming future work.

With the parameters given in Table II the values of the baryon number sum rules for u and d are: 1.9998 and 1.0003, respectively. The momentum at the initial scale adds up to 1.0016. For Set II we imposed the additional normalization condition:

$$\int_0^1 dX E_q(X, t = 0) = \kappa^q, \quad (27)$$

the experimental values of κ^q , $q = u, d$ being given in Eq. (23), while our fitted values were 1.6715 and -2.0309, for u and d respectively. The comparison with the PDF parametrization of Ref. [50] is shown in Fig. 6.

The parameters β_1 , β_2 , p_1 and p_2 , in Set I, and all parameters defining E in Set II (Eq. (16)), were fitted to the nucleon electric and magnetic form factors, Eqs. (12), with the values of M_X^q , λ^q , and α^q fixed as in Table II.

In Table III we list the values of the parameters for Set I, with their corresponding 1- σ errors (which for 6 parameters corresponds to $\Delta\chi^2 = 7.04$). The error band on the form factors resulting from the 1- σ errors on the parameters is displayed in Figs. 3, 4 and 5.

Flavor	β_1 (GeV $^{-2}$)	β_2 (GeV $^{-2}$)	p_1	p_2
u	1.9263 ± 0.0439	3.0792 ± 0.1318	0.720 ± 0.028	0.528 ± 0.031
d	1.5707 ± 0.0368	1.4316 ± 0.0440	0.720 ± 0.028	0.528 ± 0.031

TABLE III: Parameters fixing the t behavior of the GPD forms given in Set I (Eqs. (13,14)). The subscript 1(2) is for function $H^q(E^q)$, for each flavor.

In Table IV we show the values of β_1 , β_2 , p_1 and p_2 for Set II. We do not present their corresponding errors because due to the additional number of parameters in this variant

of the parametrization, the fit tends to be over-determined, and therefore not completely quantitative. This problem can be in principle circumvented either with an increased flow of new data from DVCS experiments, or by reducing the number of parameters by keeping some of their values fixed. While these strategies can be addressed in the future, we consider variant II of our fit as an indicative measure of the model dependence of the E component.

Flavor	β_1 (GeV $^{-2}$)	β_2 (GeV $^{-2}$)	p_1	p_2
u	1.9567	0.1767	0.742	0.270
d	1.5896	3.2866	0.742	0.270

TABLE IV: Parameters fixing the t behavior of the GPD forms given in Set II (Eqs. (15,16)). The subscript 1(2) is for function $H^q(E^q)$, $q = u, d$.

Additional parameters in Eqs. (15,16) are given by: $\widetilde{M}_{X_u}^{II} = 1.5780$ GeV, $\widetilde{M}_{X_d}^{II} = 0.3902$ GeV, $\widetilde{\lambda}_u^{II} = 0.2678$ GeV, $\widetilde{\lambda}_d^{II} = 0.9589$ GeV, $\widetilde{\alpha}_u^{II} = 0.005381$, $\widetilde{\alpha}_d^{II} = 0.7501$. Despite the larger number of parameters, the overall agreement with the data is not significantly different from Set I: the small t shape of the G_{M_n} data seems to be better reproduced, due to the increased flexibility, whereas with Set I one obtains a slightly better description at large t .

B. $\zeta = 0$ GPDs for u and d quarks

Our results for the GPDs are presented in Figs. 7, 8, 9, 10, and 11, respectively. In Fig. 7 we show H_u and H_d plotted vs. X at different values of t for the parameters in Set I (results for Set II are within the 2% error band shown in the figure). Plots for E_u and $-E_d$ are shown in Fig. 8 for Set I. In Fig. 9 we display results for E_u and E_d , for both Set I and Set II. Differently from H , in this case there is a much bigger discrepancy in the shape of the curves at the initial scale, Q_0^2 , due to the fact that the constraint from the PDFs is missing in this case. As will be shown later on, however, PQCD evolution reduces substantially this discrepancy.

In Fig. 10 we show the separate contributions to H_u of the diquark, $G_{M_X}^\lambda$, Eq. (17), and Regge terms, $R = X^{-\alpha-\beta(1-X)^{p_1 t}}$, respectively, at the fixed values of $t = -0.08$ GeV 2 , and $t = -1.8$ GeV 2 . From the figure it appears clearly that the form of the GPDs is determined by the diquark shape, with an “envelope” provided by the Regge term.

We reiterate that we did not attempt at guiding the values for the parameters in our Regge motivated term, based on results from soft hadron interactions phenomenology, as done instead in Ref. [13] and Ref. [14], respectively. Therefore, our final parametrization, does not depend entirely on the Regge or diquark behaviors in either the low or large X regions, but on a mixture of both.

In Fig. 11 and Fig. 12 we show the importance of the Regge term, in a quantitative fit of PDFs. In Fig. 11 the u -valence distribution, $u_v(X, Q^2)$ for our full parametrization, including both the Regge and quark-diquark term (see Eqs. (13), and (15)), is compared to both the PDF fit of Ref. [50], and to fits performed by excluding the Regge term, at $Q^2 = 5$ GeV². The quality of the “non-Regge” type fits is similar to those performed *e.g.* in [43] and [27], however it is clear that the diquark fit alone does not provide hard enough distributions at low X . This result is also independent from whether one relaxes the constraints from the baryon number and momentum sum rules. We reiterate that the term, $X^{-\alpha}$ which is essential in obtaining the argument at low X , is also necessary in order to obtain the correct value of the baryon sum rule. To test this we performed weighted fits to the low X region without the Regge term. By forcing the model to fit accurately at low X resulted in a large mismatch at larger X . Similar results are obtained from other variants of the diquark model. We conclude that the diquark model is not apt to reproduce the low X behavior, and the baryon sum rule which is in turn fundamental for a quantitative fit of GPDs from the nucleon form factors. Fig. 12 emphasizes the low X region on a logarithmic scale. It is shown in particular, how the final result (full curve) is determined by both contributions of our Regge-motivated term (thick dotted curve), and the diquark model term (dashed curve). Our fit curve is shown to be in relatively good agreement with the term: $X^{-\alpha' - \beta' t}$, where α' and β' take values consistent with Regge determinations of soft hadronic cross sections (shaded area in the figure). The interplay between the diquark model and the Regge term explains why the values of the “Regge” parameters in our fit differ sensibly from the results from hadronic cross sections, nevertheless giving an accurate description of the low X and low t regions.

Both recent parametrizations from Ref. [13] and Ref. [14], are compared with ours for $H^{u(d)}$ in Fig. 13, and in Fig. 14, respectively. A similar comparison for $E^{u(d)}$ is performed in Figs. 15 and 16. The results presented in the figure were obtained by evolving to Leading Order (LO) the parametrizations at the initial scale $Q_0^2 \approx 0.1$ GeV² to the values of $Q^2 = 1$ GeV², and $Q^2 = 4$ GeV², where the parametrizations from [13] and [14] were respectively given. We reiterate that in principle higher order effects are important especially considering the low values of the scale, and that PQCD evolution for GPDs involves many more subtleties that already appear at NLO (see *e.g.* [7] and references therein). Lacking however, any knowledge from experiment, it is still important to take into account the effects of PQCD evolution, as indicators of the general trend followed by GPDs.

At low t we notice a very good agreement in both H^u and H^d among all three approaches, essentially because the GPDs tend to the forward limit constrained by PDFs, whereas a disagreement appears in the large t behavior. This is clearly an effect of perturbative evolution that sets in earlier in our case with respect to Refs. [13, 14], and that does not

conserve the form of the initial function, as also noticed in [13]. One can gain insight on this point, as first observed in the preliminary study of Ref. [12], by plotting the quantity:

$$\langle X^q(t) \rangle = \frac{\int_0^1 dX X H^q(X, t)}{\int_0^1 dX H^q(X, t)} \equiv \frac{1}{F_1^q(t)} \int_0^1 dX X H^q(X, t), \quad (28)$$

representing the average value of X contributing respectively, to the u and d components of the nucleon form factors, F_1^u and F_1^d (Eq. (11)). In Fig. 17 we plot $\langle X^q(t) \rangle$ at $Q^2 \equiv Q_0^2$. The contribution to the proton form factor is obtained as:

$$\langle X^p(t) \rangle = \frac{2}{3} \frac{F_1^u}{F_1^p} \langle X^u(t) \rangle - \frac{1}{3} \frac{F_1^d}{F_1^p} \langle X^d(t) \rangle. \quad (29)$$

Notice that the total momentum carried by the valence u and d quarks is instead given by:

$$\langle X \rangle = 2\langle X^u(0) \rangle + \langle X^d(0) \rangle. \quad (30)$$

From Fig. 17 one can see that at $Q^2 = Q_0^2$, $\langle X \rangle = 1$, *i.e.* all the momentum is carried by the valence quarks. PQCD evolution implies that:

$$\langle X^q(t, Q^2) \rangle = \langle X^q(t, Q_0^2) \rangle [\alpha_s(Q^2)/\alpha_s(Q_0^2)]^{d_2}, \quad (31)$$

where α_s is the strong coupling constant, and the anomalous dimension yields $d_2 = 0.4267$. One can therefore observe that although larger values of X tend to dominate the form factor as t increases, the effect of PQCD evolution reduces the large X components by a Q^2 -dependent shift. This effect explains the discrepancies in the curves at $-t = 5 \text{ GeV}^2$ in Figs. 12,13,14,15.

A similar behavior is observed for $E^{u(d)}$, although all parametrizations tend to quantitatively differ also at low t , since they are not constrained by the PDFs.

IV. PHENOMENOLOGY

With the results of a precise fit at hand, we can address some issues in the phenomenology of GPDs at zero skewness.

A. Coordinate Space Observables

A most interesting aspect is the relation with the nucleon Impact Parameter dependent PDFs (IPPDFs), $q(X, \mathbf{b})$, related via Fourier transformation to $H^q(X, t \equiv -\Delta_\perp^2)$ [4]:

$$q(X, \mathbf{b}) = \int d^2\Delta e^{i\mathbf{b}\cdot\Delta} H^q(X, t), \quad (32)$$

$q(X, \mathbf{b})$ is the probability of finding a quark in the proton carrying momentum fraction X , at impact parameter \mathbf{b} .

The quark's average impact parameter can be derived as:

$$\langle b_q^2(X) \rangle = \frac{\int d^2\mathbf{b} q(X, \mathbf{b}) b^2}{\int d^2\mathbf{b} q(X, \mathbf{b})} = 4 \left. \frac{\partial}{\partial t} \log H^q(X, t) \right|_{t=0}, \quad (33)$$

from which an average ‘‘interparton distance’’ [54] can be defined as:

$$\langle y_q^2(X) \rangle = \frac{\langle b_q^2(X) \rangle}{(1-X)^2}. \quad (34)$$

Similarly, E^q can be interpreted in terms of a distribution function in a transversely polarized target, through:

$$q^X(X, \mathbf{b}) = q(X, \mathbf{b}) - \frac{b_y}{M} \frac{\partial}{\partial \mathbf{b}^2} \int d^2\Delta e^{i\mathbf{b}\cdot\Delta} E^q(X, t), \quad (35)$$

where polarization is along the x axis and b_y is the component of \mathbf{b} along the y axis. $q^X(X, \mathbf{b})$ measures the probability of finding a quark carrying momentum fraction X in the transversely polarized proton, at impact parameter \mathbf{b} . The average shift in the quark's distance along the y -axis for polarization along the x -axis direction is obtained from Eq. (35) as [4]:

$$\langle b_q^y(X) \rangle = \frac{\int d^2\mathbf{b} q^X(X, \mathbf{b}) b_y}{\int d^2\mathbf{b} q^X(X, \mathbf{b})} = \frac{1}{2M} \frac{E^q(X, 0)}{H^q(X, 0)}. \quad (36)$$

The shift relative to the spectator quarks is obtained analogously to Eq. (34) as:

$$\langle s_q(X) \rangle = \frac{\langle b_q^y(X) \rangle}{1-X}. \quad (37)$$

The average interparton distances, and the transverse shifts are shown in Fig. 18, and Fig. 19, respectively.

In our approach the radii are a result of the fitting procedure rather than an additional constraint as in Refs. [13, 14]. We studied the role of the Regge-type and diquark terms from Eq. (5). Because of the factorized form, $\langle y_q^2(X) \rangle$ can be expressed in fact as the sum of the two terms. We find a larger than intuitively expected contribution of the diquark term to both the d and u quarks interparton distances. Notice that the interparton distances are subject to PQCD evolution. In Fig. 18 we display results at our initial low scale, Q_0^2 . The effect of evolution is shown by plotting the total interparton distance – including both Regge and diquarks terms – at $Q^2 = 4 \text{ GeV}^2$. One can see that the interparton distances tend to decrease with Q^2 , as the term $\partial H/\partial t$ in Eq. (33) evolves more steeply than H .

The total radius squared of the nucleon is obtained by considering:

$$\langle r_1^{q^2} \rangle = \left. \frac{\int dX q(X) \langle b_q^2(X) \rangle}{F_1^q(t)} \right|_{t=0} = 4 \left. \frac{\partial}{\partial t} \log F_1^q(t) \right|_{t=0}, \quad (38)$$

and using isospin symmetry:

$$\langle r_1^{p2} \rangle = \frac{4}{3} \langle r_1^{u2} \rangle - \frac{1}{3} \langle r_1^{d2} \rangle \quad (39a)$$

$$\langle r_1^{n2} \rangle = -\frac{2}{3} \langle r_1^{u2} \rangle + \frac{2}{3} \langle r_1^{d2} \rangle \quad (39b)$$

The charge radii are given by:

$$\langle r_E^{p2} \rangle = \langle r_1^{p2} \rangle + \frac{3}{2} \frac{\kappa_p}{M^2} \quad (40a)$$

$$\langle r_E^{n2} \rangle = \langle r_1^{p2} \rangle + \frac{3}{2} \frac{\kappa_n}{M^2}, \quad (40b)$$

We find: $\langle r_1^{u2} \rangle = 0.654 \text{ fm}^2$, $\langle r_1^{d2} \rangle = 0.666 \text{ fm}^2$, $\langle r_1^{p2} \rangle = 0.650 \text{ fm}^2$, $\langle r_1^{n2} \rangle = 0.0078 \text{ fm}^2$. The calculated values for the total charge radii are: $\langle r_E^{p2} \rangle = 0.76 \text{ fm}^2$ and $\langle r_E^{n2} \rangle = -0.118 \text{ fm}^2$, in agreement with the experimental results. Therefore our results for the fit parameters $\alpha_q \approx 1 - 1.2$ in Eq. (5) are in line with the constraints on the Regge parameters studied in Ref. [14].

The transverse shift, s_q , (Fig. 19) constitutes in principle a test on the GPD E^q . Our results, plotted at the initial scale, show a marked difference between Set I and Set II. One should keep in mind however, that PQCD evolution largely diminishes the discrepancy.

B. Intrinsic Transverse Momentum

An observable related to transversity that can be accessed within our model, is the partons' average intrinsic transverse momentum, $\langle k_\perp^2(X) \rangle_q$. Notice that \mathbf{k}_\perp , although not Fourier conjugate to \mathbf{b} , it can be related to $q(X, \mathbf{b})$ as shown in Ref. [12].⁴ In other words, \mathbf{k}_\perp is not directly observable in DVCS type processes. However, it can be evaluated using the same input to Eq. (5), as:

$$\langle k_\perp^2(X) \rangle_q = \frac{\int d^2\mathbf{k}_\perp |\phi(k^2, \lambda^2)|^2 \mathbf{k}_\perp^2}{\int d^2\mathbf{k} |\phi(k^2, \lambda^2)|^2}, \quad (41a)$$

$$\langle k_\perp^2(X) \rangle \equiv \langle k_\perp^2(X) \rangle_p = \frac{4}{9} \langle k_\perp^2(X) \rangle_u + \frac{1}{9} \langle k_\perp^2(X) \rangle_d \quad (41b)$$

In Fig. 20 we show $\langle k_\perp^2(X) \rangle$ from our model. In order to assess the range of possible variations for this observable, we compare our evaluation with the values extracted from Refs. [13] and [14], by assuming a gaussian k_\perp dependence of the vertex functions that could originate such parametrizations. We also compare with the hypothesis originally advanced by Burkardt [55] on the form of the combined X and t dependences of the gaussian's exponent (or the

⁴ Such relation is of general validity, unrelated to non-relativistic many body theory as quoted in [8].

profile function in [13, 14]). Finally, we compare with the values used in Semi-Inclusive DIS (SIDIS) parametrizations [43, 56]. The exploratory work presented here is aimed at defining a few guidelines for future quantitative studies of the connection between GPDs and SIDIS reactions [4, 57]. In Fig. 21 we show the ratios:

$$R_{k_{max}}^{1(2)}(t) = F_{1(2)}(t, k_{max})/F_{1(2)}(t) \quad (42)$$

$$R_{X_{max}}^{1(2)}(t) = F_{1(2)}(t, X_{max})/F_{1(2)}(t) \quad (43)$$

in order to determine what k_{\perp} , and X components the form factors are dominated by. The numerators were obtained by setting the upper limit of integration in Eq. (10) to different values of $k_{\perp} \equiv k_{max}$, and $X \equiv X_{max}$, respectively. It can be clearly seen that for all values of t the form factor ratio, $R_{k_{max}}^{1(2)}(t)$, is saturated by setting $k_{max} \approx 1$ GeV (for F_2 , even larger values of k_{\perp} seem to be important). This is in turn an indication of a semi-hard distribution, as opposed to the soft gaussian forms used elsewhere. On the other side, the ratio $R_{X_{max}}^{1(2)}(t)$ clearly shows the coupling between the $X \rightarrow 1$ behavior of the GPDs and the large t behavior of the form factors.

C. Implementation of Lattice QCD Results

Lattice QCD provides the only “model independent” constraints that are necessary to parametrize GPDs at $\zeta \neq 0$. It is, however, important to illustrate the type of information that can be obtained on GPDs starting from the $\zeta = 0$ case. The $\zeta \neq 0$ case requires in addition, a more involved “deconvolution” procedure from the first three moments that will be described in a following dedicated paper [23].

Current lattice results can reproduce the dipole fall-off of the form factors up to $-t \approx 3$ GeV². However, even after performing a linear extrapolation to low values of the pion mass, such calculations overshoot the experimental results [13, 21, 22]. As a result, predictions from the lattice are at the moment characterized by a rather large uncertainty. This becomes problematic especially for the higher moments of GPDs where no comparison with experimental results can be made. In order to evaluate the impact of such uncertainty on possible extractions of GPDs, we performed a test based on a prescription proposed in [36] by Schierholz, according to which the value of the dipole mass, Λ_n , appearing in: ⁵

$$M_n(t) = \int_0^1 dX H(X, t) X^{n-1} = M_n(0) \frac{1}{\left(1 + \frac{t}{\Lambda_n^2}\right)^2}, \quad (44)$$

⁵ We reiterate that Eq. (44) is not of general validity but a result of fits to the lattice calculations of [21, 22].

can be first extracted from the lattice evaluations for $n \leq 3$, and subsequently extended to all n values by performing a fit based on a Regge motivated ansatz of the type:

$$\sqrt{\Lambda_n^2} = \frac{n - \alpha_0}{\alpha_v}. \quad (45)$$

(in Eq. (44) $H = H^u - H^d \equiv H^{u-d}$ evaluated at $Q^2 = 4 \text{ GeV}^2$). The n -dependence of the moments described above allows one to perform the anti-Mellin transform, thus obtaining GPDs, analytically. Results using Eqs. (44,45), are compared with the evaluations from our analysis at $Q^2 = 4 \text{ GeV}^2$, in Fig. 22. The band in the figure includes the estimate of the lattice error. One can observe a good agreement with both our results and other current parametrizations for the H^u at $t \lesssim 2 \text{ GeV}^2$. The agreement however, deteriorates at lower t for the d -quark. We therefore conclude that within the range of t shown in the figure, it is acceptable to use current lattice results in order to extend our analysis of the extraction of GPDs at $\zeta \neq 0$.

V. CONCLUSIONS AND OUTLOOK

In this paper we proposed a fully quantitative physically motivated parametrization of generalized parton distributions that is constructed directly from a covariant model for the quark-nucleon scattering amplitude. Therefore, we do not implement a specific form for the forward limit given by the parton distribution functions of DIS, but we obtain that limit from fitting directly to the valence contribution to DIS data. This allows us in particular to better study the role of Regge-type exchanges, that are disengaged, in our case, from the specific form of parton distributions. The other constraints defining our parametrization at zero skewness are provided by the electric and nucleon form factor data.

The advantages of this approach are that on one side, using the same initial formalism, we can predict additional quantities such as the the unintegrated, k_\perp -dependent, parton distribution functions. This degree of flexibility is desirable in view of both future interpretations of both coordinate space observables, and of transversity. Furthermore, analyzing directly the vertex structure of the scattering amplitude allows us to easily extended our predictions to the non-zero skewness case. This can be, in fact, obtained by extending the range of the kinematical variables in our expressions for the quark scattering dominated region, and by considering separately the $X < \zeta$ region where a quark-antiquark pair from the initial proton participates in the scattering process. Additional constraints need however to be provided by the higher, ζ -dependent, moments of the GPDs. These are in principle available from recent lattice calculations but are necessarily fraught with uncertainties. Here were able to assess the impact of such ambiguities on the extraction of GPDs. We conclude that current extrapolated lattice values can be used for $t \lesssim 2 \text{ GeV}^2$. A detailed description

of the ζ dependent parametrization is given in a forthcoming paper.

With this type of parametrization in hand we can on one side provide predictions for both recent [41, 58] and future DVCS measurements at Jefferson Lab. On the other, our approach is geared towards providing a practical and more flexible method to reconstruct generalized parton distributions from their first few moments.

Acknowledgments

We thank S. J. Brodsky, F. Llanes-Estrada and P. Kroll for useful comments. This work is supported by the U.S. Department of Energy grant no. DE-FG02-01ER41200 and NSF grant no.0426971.

APPENDIX A: CONNECTION BETWEEN DIFFERENT SETS OF KINEMATICAL VARIABLES

By defining [2]: $x = (k^+ + k'^+)/ (P^+ + P'^+)$, $\xi = \Delta^+ / (P^+ + P'^+)$, and t , the following mappings with the kinematical variables defined in the paper obtain: The regions $-\xi < x < \xi$ and $\xi < x < 1$ are mapped into $0 < X < \zeta$ and $\zeta < X < 1$ respectively, via:

$$X = \frac{x + \xi}{1 + \xi} \quad (\text{A1a})$$

$$\zeta = \frac{2\xi}{1 + \xi}, \quad (\text{A1b})$$

while the region $-1 < x < -\xi$ maps into $\zeta < X < 1$, via :

$$X = \frac{-x + \xi}{1 + \xi} \quad (\text{A2a})$$

$$\zeta = \frac{2\xi}{1 + \xi} \quad (\text{A2b})$$

APPENDIX B: ANALYTIC EXPRESSIONS FOR THE NUCLEON'S RADIUS

We give the analytic expressions for $\langle b_q^2(X) \rangle$, obtained from the factorized form in Eq. (13):

$$\begin{aligned} \langle b_q^2(X) \rangle &= 4 \left. \frac{\partial}{\partial t} \log H^q(X, t) \right|_{t=0} \\ &= -\frac{1}{2\Delta} \left[\frac{\partial \ln G_{MX}^\lambda}{\partial \Delta} + \frac{\partial \ln R}{\partial \Delta} \right] \Bigg|_{\Delta=0} \\ &= (\langle b_q^2(X) \rangle_G + \langle b_q^2(X) \rangle_R) \frac{1}{q(X)} \\ &= \frac{3}{5} \frac{1 - X}{(-M^2 + \frac{X}{1-X} M_X^{q^2} - \lambda_q^2)} - \beta_1 (1 - X)^{p_1} \log X \end{aligned} \quad (\text{B1})$$

with $\Delta = \sqrt{-t}$, G_{MX}^λ given in Eq.(17), and $R = X^{-\alpha - \beta_1(1-X)^{p_1} t}$.

-
- [1] D. Muller, D. Robaschik, B. Geyer, F. M. Dittes and J. Horejsi, Fortsch. Phys. **42**, 101 (1994)
 - [2] X. D. Ji, Phys. Rev. D **55**, 7114 (1997)
 - [3] A. V. Radyushkin, Phys. Rev. D **56**, 5524 (1997)
 - [4] M. Burkardt, Int. J. Mod. Phys. A **18**, 173 (2003); *ibid* Phys. Rev. D **62**, 071503 (2000) [Erratum-*ibid*. D **66**, 119903 (2002)].
 - [5] W.-M. Yao et al., J. Phys. G **33**, 1 (2006), “2006 Review of Particle Physics”.
 - [6] A. V. Belitsky, D. Mueller and A. Kirchner, Nucl. Phys. B **629**, 323 (2002)

- [7] M. Diehl, Phys. Rept. **388**, 41 (2003).
- [8] A. V. Belitsky and A. V. Radyushkin, Phys. Rept. **418**, 1 (2005)
- [9] P. Stoler, Phys. Rev. D **65**, 053013 (2002)
- [10] A. Gardestig, A. P. Szczepaniak and J. T. Londergan, Phys. Rev. D **68**, 034005 (2003)
- [11] A.V. Afanasev, hep-ph/9808291; hep-ph/9910565.
- [12] S. Liuti and S. K. Taneja, Phys. Rev. D **70**, 074019 (2004)
- [13] M. Diehl, T. Feldmann, R. Jakob and P. Kroll, Eur. Phys. J. C **39**, 1 (2005)
- [14] M. Guidal, M. V. Polyakov, A. V. Radyushkin and M. Vanderhaeghen, Phys. Rev. D **72**, 054013 (2005)
- [15] A. V. Radyushkin, arXiv:hep-ph/0101225.
- [16] M. Vanderhaeghen, M. Guidal and P. Guichon, “VGG code”, *private communication*.
- [17] D. Mueller and A. Schafer, Nucl. Phys. B **739**, 1 (2006)
- [18] V. Guzey and M. V. Polyakov, Eur. Phys. J. C **46**, 151 (2006)
- [19] G. C. Fox, Nucl. Phys. B **131**, 107 (1977).
- [20] F. J. Yndurain, Phys. Lett. B **74**, 68 (1978).
- [21] M. Gockeler *et al.* [QCDSF Collaboration], Phys. Rev. Lett. **92**, 042002 (2004); M. Gockeler *et al.*, Nucl. Phys. Proc. Suppl. **153**, 146 (2006) [arXiv:hep-lat/0512011]
- [22] P. Hagler, J. Negele, D. B. Renner, W. Schroers, T. Lippert and K. Schilling [LHPC collaboration], Phys. Rev. D **68**, 034505 (2003).
- [23] S.Ahmad, H.Honkanen, S.Liuti and S.K. Taneja, “*Generalized Parton Distributions from Hadronic Observables: $\zeta \neq 0$* ”, in preparation.
- [24] K. J. Golec-Biernat and A. D. Martin, Phys. Rev. D **59**, 014029 (1999)
- [25] S. J. Brodsky, M. Diehl and D. S. Hwang, Nucl. Phys. B **596**, 99 (2001)
- [26] H. Meyer and P. J. Mulders, Nucl. Phys. A **528**, 589 (1991).
- [27] W. Melnitchouk, A. W. Schreiber and A. W. Thomas, Phys. Rev. D **49**, 1183 (1994)
- [28] S. Liuti and S. K. Taneja, Phys. Rev. C **72**, 034902 (2005)
- [29] S. J. Brodsky, F. E. Close and J. F. Gunion, Phys. Rev. D **8**, 3678 (1973).
- [30] A. P. Szczepaniak and J. T. Londergan, arXiv:hep-ph/0604266.
- [31] J. Bolz and P. Kroll, Z. Phys. A **356**, 327 (1996)
- [32] M. Diehl, T. Feldmann, R. Jakob and P. Kroll, Nucl. Phys. B **596**, 33 (2001) [Erratum-ibid. B **605**, 647 (2001)]
- [33] A. Airapetian *et al.* [HERMES Collaboration], Phys. Rev. Lett. **87**, 182001 (2001)
- [34] S. Stepanyan *et al.* [CLAS Collaboration], Phys. Rev. Lett. **87**, 182002 (2001)
- [35] S. J. Brodsky and F. J. Llanes-Estrada, Eur. Phys. J. C **46**, 751 (2006)
- [36] G.Schierholz, in *GPD 2006: Workshop on Generalized Parton Distributions*, June 2006, ECT* Trento, Italy – <http://gpd.gla.ac.uk/gpd2006/index.php>; and *private communication*.
- [37] A. Acha *et al.* [HAPPEX collaboration], arXiv:nucl-ex/0609002.
- [38] C. R. Ji, Y. Mishchenko and A. Radyushkin, Phys. Rev. D **73**, 114013 (2006); H. M. Choi, C. R. Ji and L. S. Kisslinger, Phys. Rev. D **64**, 093006 (2001)
- [39] V. Barone, *et al.*, hep-ex 0505054.
- [40] M. Glück *et al.*, Z. Phys. **C 41** (1989) 667; *ibid* Z. Phys. **C 48** (1990) 471.
- [41] C. Munoz Camacho *et al.* [Jefferson Lab Hall A Collaboration], arXiv:nucl-ex/0607029.
- [42] J. Pumplin, AIP Conf. Proc. **792**, 50 (2005)
- [43] R. Jakob, P. J. Mulders and J. Rodrigues, Nucl. Phys. A **626**, 937 (1997)
- [44] L. E. Price, J. R. Dunning, M. Goitein, K. Hanson, T. Kirk and R. Wilson, Phys. Rev. D **4** (1971) 45; G. G. Simon, C. Schmitt, F. Borkowski and V. H. Walther, Nucl. Phys. A **333**,

- 381 (1980).
- [45] G. Hohler, E. Pietarinen, I. Sabba Stefanescu, F. Borkowski, G. G. Simon, V. H. Walther and R. D. Wendling, Nucl. Phys. B **114**, 505 (1976); E. J. Brash, A. Kozlov, S. Li and G. M. Huber, Phys. Rev. C **65**, 051001 (2002)
 - [46] T. Eden *et al.*, Phys. Rev. C **50**, 1749 (1994); I. Passchier *et al.*, Phys. Rev. Lett. **82**, 4988 (1999); C. Herberg *et al.*, Eur. Phys. J. A **5**, 131 (1999); J. Golak, G. Ziemer, H. Kamada, H. Witala and W. Gloeckle, Phys. Rev. C **63**, 034006 (2001); R. Madey *et al.* [E93-038 Collaboration], Phys. Rev. Lett. **91**, 122002 (2003); G. Warren *et al.* [Jefferson Lab E93-026 Collaboration], Phys. Rev. Lett. **92**, 042301 (2004); R. Schiavilla and I. Sick, Phys. Rev. C **64**, 041002 (2001); D. Rohe *et al.*, Phys. Rev. Lett. **83**, 4257 (1999).
 - [47] G. Kubon *et al.*, Phys. Lett. B **524**, 26 (2002); H. Anklin *et al.*, Phys. Lett. B **336**, 313 (1994); H. Anklin *et al.*, Phys. Lett. B **428**, 248 (1998); A. Lung *et al.*, Phys. Rev. Lett. **70**, 718 (1993); W. Xu *et al.*, Phys. Rev. Lett. **85**, 2900 (2000); W. Xu *et al.* [Jefferson Lab E95-001 Collaboration], Phys. Rev. C **67**, 012201 (2003); S. Rock *et al.*, Phys. Rev. Lett. **49**, 1139 (1982).
 - [48] M. K. Jones *et al.* [Jefferson Lab Hall A Collaboration], Phys. Rev. Lett. **84**, 1398 (2000); O. Gayou *et al.* [Jefferson Lab Hall A Collaboration], Phys. Rev. Lett. **88**, 092301 (2002); T. Pospischil *et al.* [A1 Collaboration], Eur. Phys. J. A **12**, 125 (2001); B. D. Milbrath *et al.* [Bates FPP collaboration], Phys. Rev. Lett. **80**, 452 (1998) [Erratum-ibid. **82**, 2221 (1999)]
 - [49] J. J. Kelly, Phys. Rev. C **70**, 068202 (2004).
 - [50] S. Alekhin, Phys. Rev. D **68**, 014002 (2003)
 - [51] J. Pumplin, D. R. Stump, J. Huston, H. L. Lai, P. Nadolsky and W. K. Tung, JHEP **0207**, 012 (2002)
 - [52] R. S. Thorne, A. D. Martin and W. J. Stirling, arXiv:hep-ph/0606244.
 - [53] A. W. Schreiber, A. W. Thomas and J. T. Londergan, Phys. Rev. D **42**, 2226 (1990).
 - [54] D. E. Soper, Phys. Rev. D **15**, 1141 (1977).
 - [55] M. Burkardt, Phys. Rev. D **66**, 114005 (2002).
 - [56] M. Anselmino, M. Boglione, U. D'Alesio, A. Kotzinian, F. Murgia and A. Prokudin, Phys. Rev. D **72**, 094007 (2005) [Erratum-ibid. D **72**, 099903 (2005)]
 - [57] M. Diehl and Ph. Hagler, Eur. Phys. J. C **44**, 87 (2005).
 - [58] H. Avakian, *private communication*.

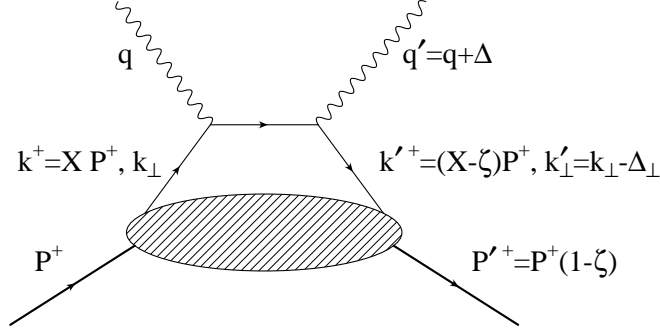


FIG. 1: Amplitude for DVCS at leading order in Q^2 . The light-cone coordinates for the active quarks and nucleons are explicitly written.

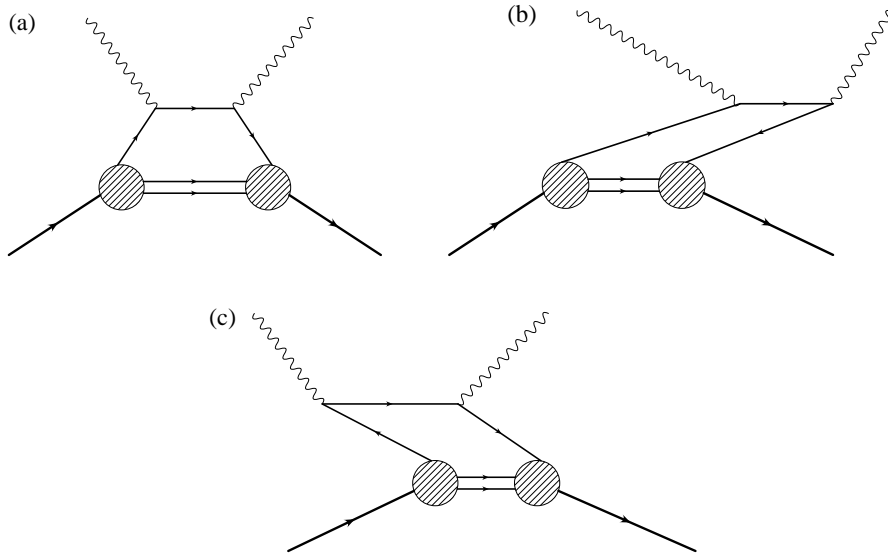


FIG. 2: Time ordered diagrams for DVCS: **(a)** dominant contribution in $X > \zeta$ region; **(b)** a $q\bar{q}$ pair is first produced from the nucleon and subsequently interacts with the photons. This process dominates the $X < \zeta$ region; **(c)** the initial photon splits into a $q\bar{q}$ pair that interacts with the hadronic system. The crossed-terms where two of the particles in the same class are switched, are not shown in the figure.

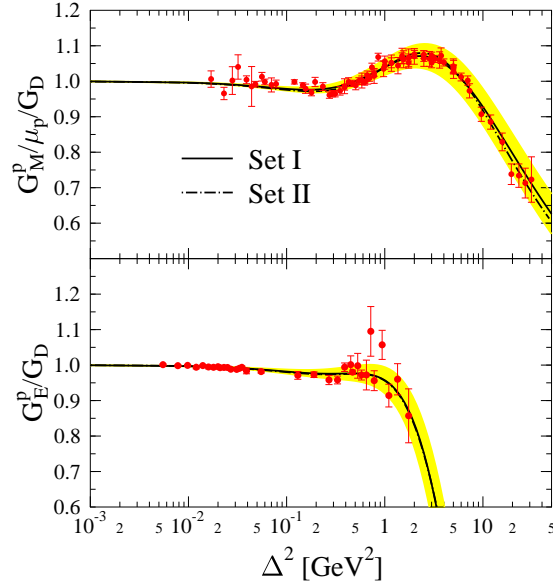


FIG. 3: The proton magnetic and electric form factors, G_M^p and G_E^p , respectively, divided by the dipole, $G_D = 1/(1 + Q^2/0.71 \text{ GeV}^2)^2$, plotted vs. Δ^2 . Experimental data from [44] (G_{E_p}); [45] (G_{M_p}). The full line was obtained using parametrization I, Eqs. (13,14); the dot-dashed line corresponds to parametrization II, Eqs. (15,16).

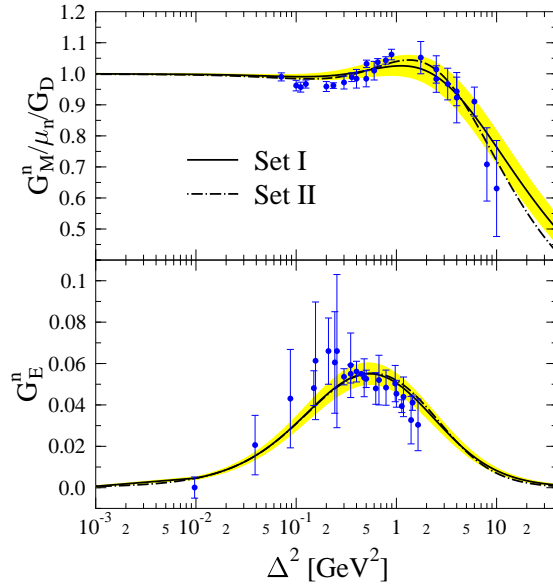


FIG. 4: The neutron magnetic form factor, G_M^n , divided by the dipole, $G_D = 1/(1 + \Delta^2/0.71 \text{ GeV}^2)^2$, and electric form factor, G_E^n , respectively, plotted vs. Δ^2 . Experimental data from [47] (G_{M_n}) and [46] (G_{E_n}). Notation as in Fig. 3.

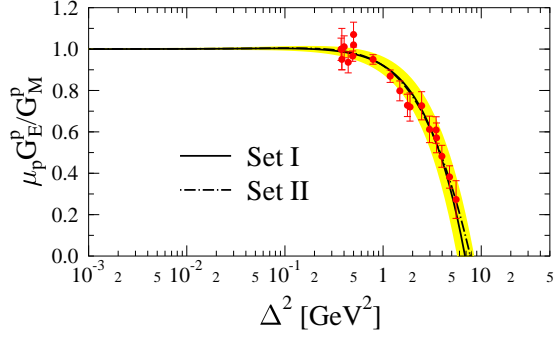


FIG. 5: The ratio of proton electric and magnetic form factors, $\mu_p G_M^p(t)/G_E^p(t)$. Experimental data from [48]. Notation as in Fig. 3.

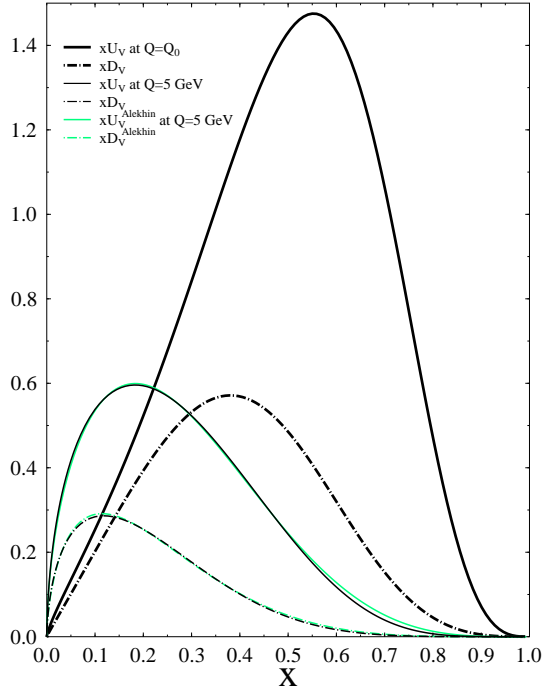


FIG. 6: (color online) Parton distribution functions, $Xu_v(X)$ and $Xd_v(X)$ plotted vs. X , at the initial scale, $Q_0 = 0.3$ GeV, and at $Q = 5$ GeV. The parton distributions parameters, including the value of the initial scale were obtained directly from our fit. The fitted parameters are: M_X , λ , α for both parametrization I and II. Our results are shown together with the LO set of Alekhin PDFs [50] used in the fit.

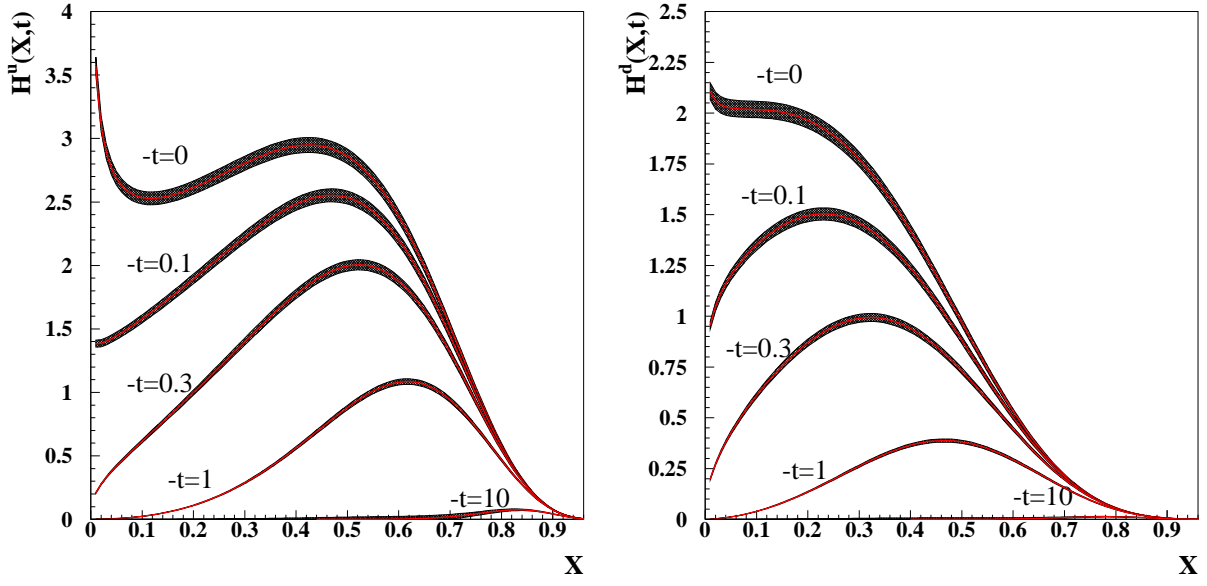


FIG. 7: The generalized parton distributions, H_u (left panel) and H_d (right panel) obtained from Parametrization I, defined by Eq. (13), plotted vs. X at $-t = 0, 0.1, 0.3, 1, 10 \text{ GeV}^2$, respectively, at the initial scale $Q_0^2 = 0.09 \text{ GeV}^2$. Results for Parametrization II, Eq. (15) are very similar. They are included within the 2% band displayed in the figure

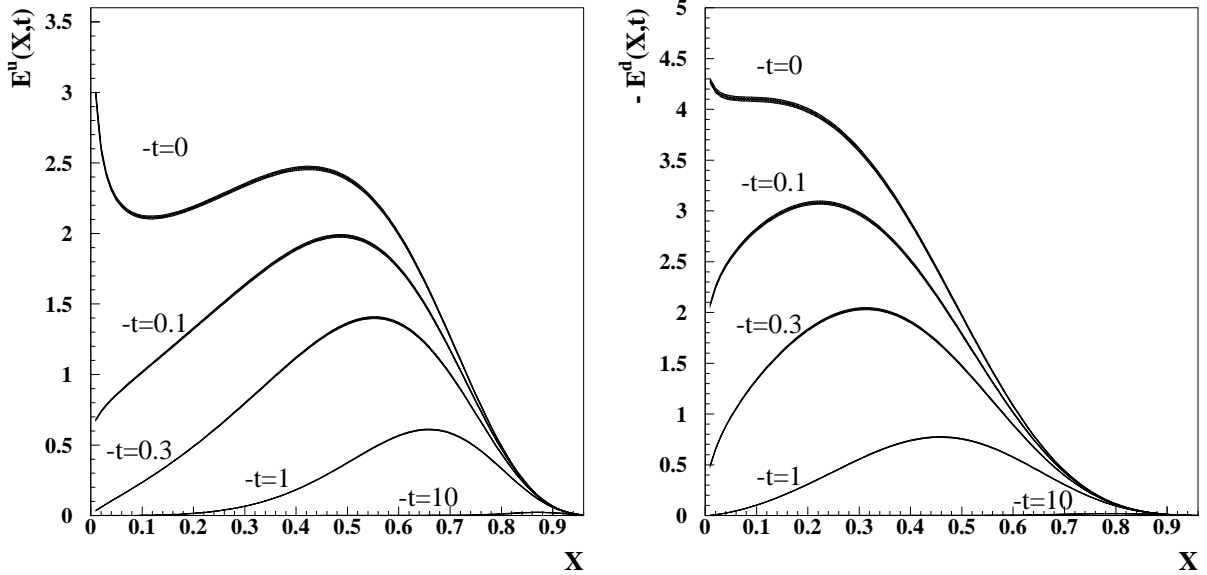


FIG. 8: The generalized parton distributions, E_u (left panel) and $-E_d$ (right panel) obtained from Eq. (14) – Parametrization I – plotted vs. X at $-t = 0, 0.1, 0.3, 1, 10 \text{ GeV}^2$, respectively, at the initial scale $Q_0^2 = 0.09 \text{ GeV}^2$.

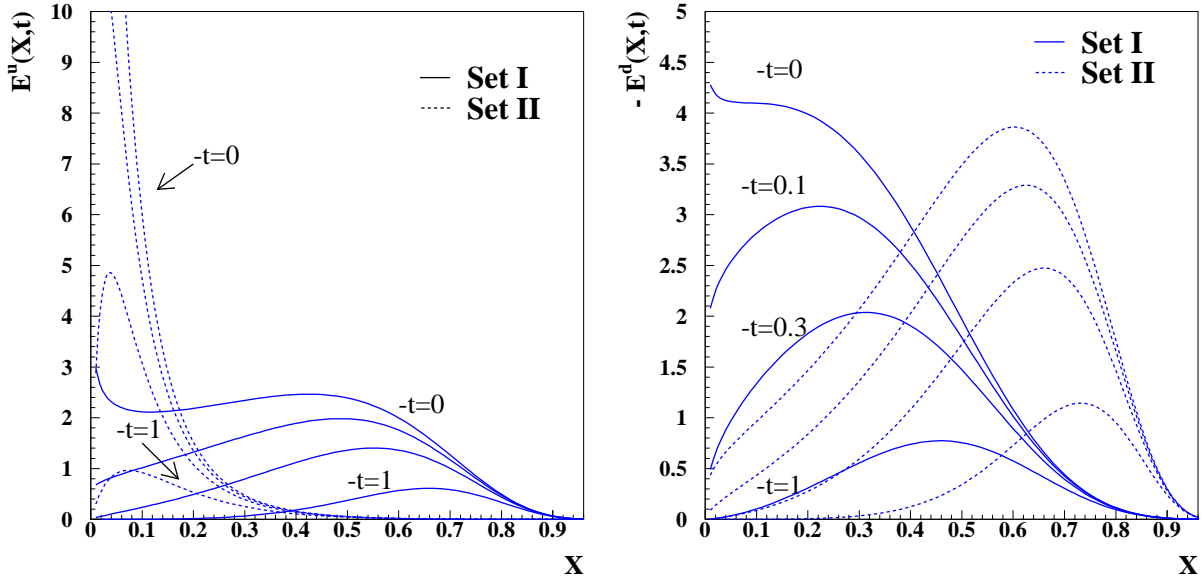


FIG. 9: Left panel: E_u obtained with Parametrization I (full lines) and II (dashed lines), respectively, for different values of $-t$: $-t = 0, 0.1, 0.3, 1$ GeV^2 , at the initial scale $Q_0^2 = 0.09$ GeV^2 . Right panel: the same for $-E_d$.

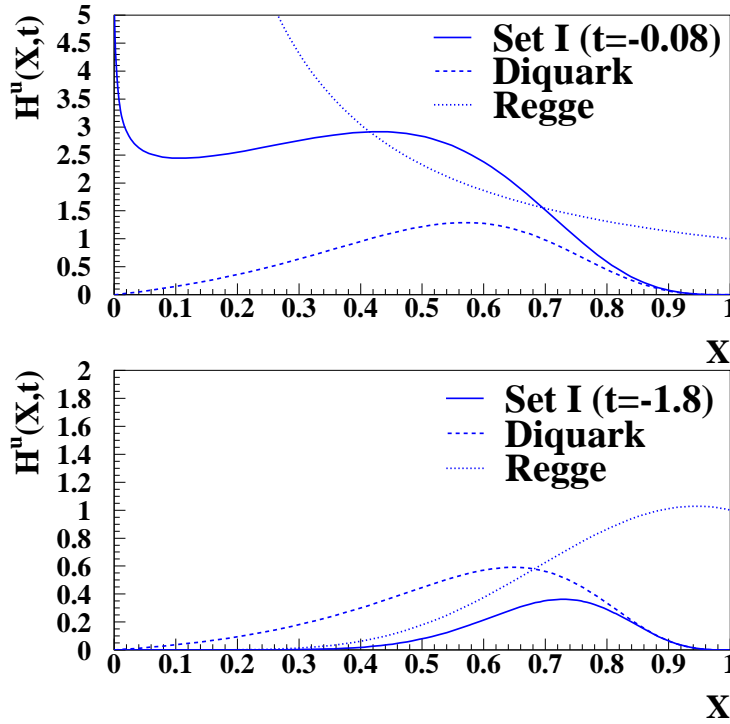


FIG. 10: Contributions to H_u of the diquark term: $G_{M_X}^\lambda$, Eq. (17), and of the Regge terms: $R = X^{-\alpha-\beta(1-X)^{p_1 t}}$, respectively, at $t = -0.08$ GeV^2 (top) and $t = -1.8$ GeV^2 (bottom). From the figure one can see that the form of the GPDs is determined by the diquark shape, with an “envelope” provided by the Regge term.

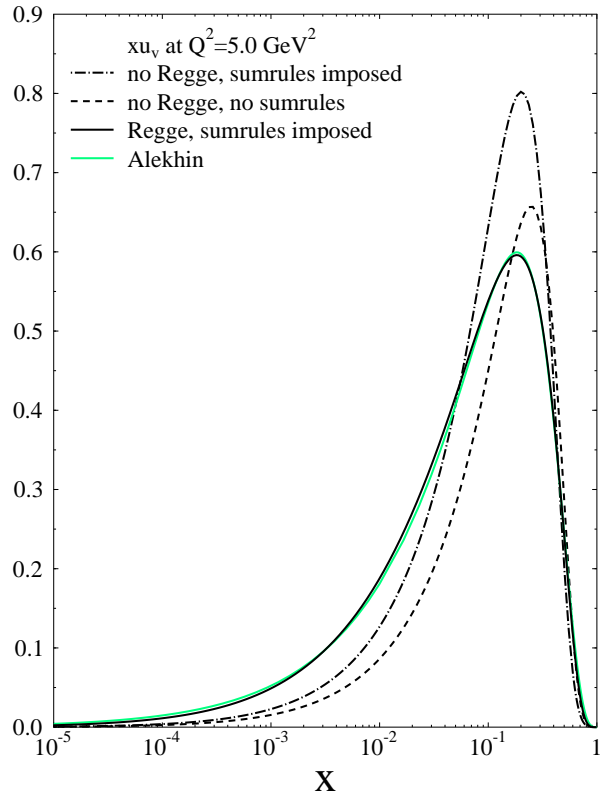


FIG. 11: (color online) Role of the Regge-motivated term, $R = X^{-\alpha-\beta(1-X)^{p_1 t}}$, in H_u , in order to accomplish a quantitative fit of the PDF $u_v(X, Q^2)$.

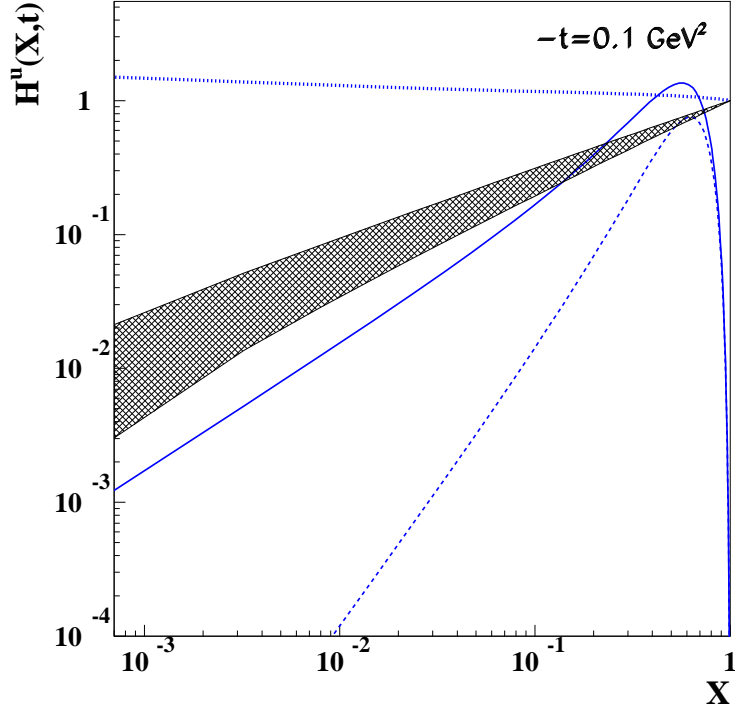


FIG. 12: (color online) Role of Regge-motivated term in Eqs. (13,15). Thick dotted line: $X^{-\alpha-\beta(1-x)^{p_1}t}$, with fit parameters from Tables II and III; dashed line: quark-diquark term, $G_{M_X}^\lambda$; Full line: total value, Eqs. (13,15). Shaded area: Regge term: $X^{-\alpha'-\beta't}$, with fit parameters from phenomenological Regge fits. All curves were calculated at $t = -0.1 \text{ GeV}^2$.

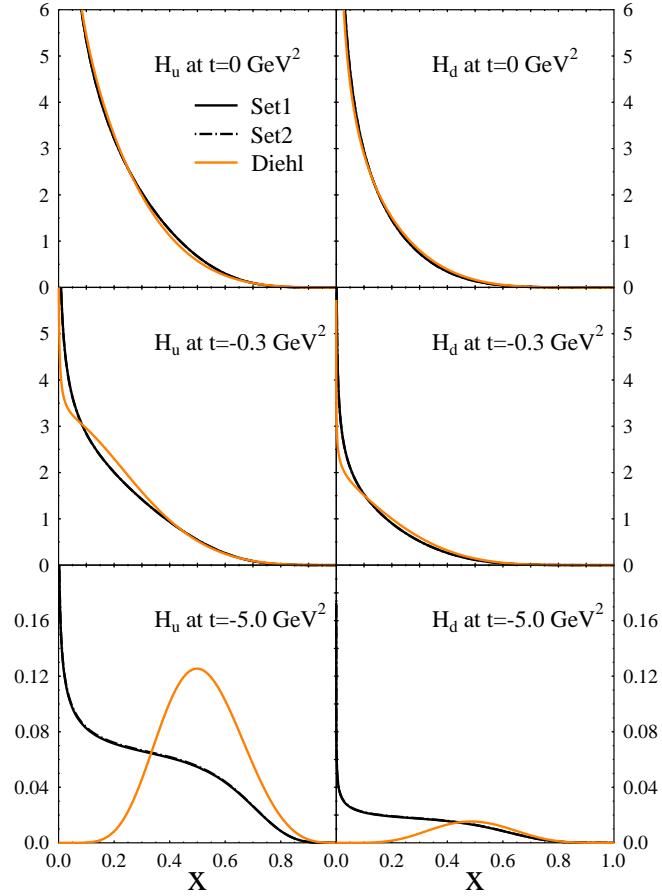


FIG. 13: (color online) Comparison with the quantitative extraction of GPDs from data from Ref. [13]. H_u (left) and H_d (right) as a function of X for $-t = 0, 0.3, 5 \text{ GeV}^2$, for our Parametrizations I and II, respectively evolved at $Q^2 = 4 \text{ GeV}^2$ used in Ref. [13] While a clear agreement is seen at low values of t , this becomes worse at larger values of t .

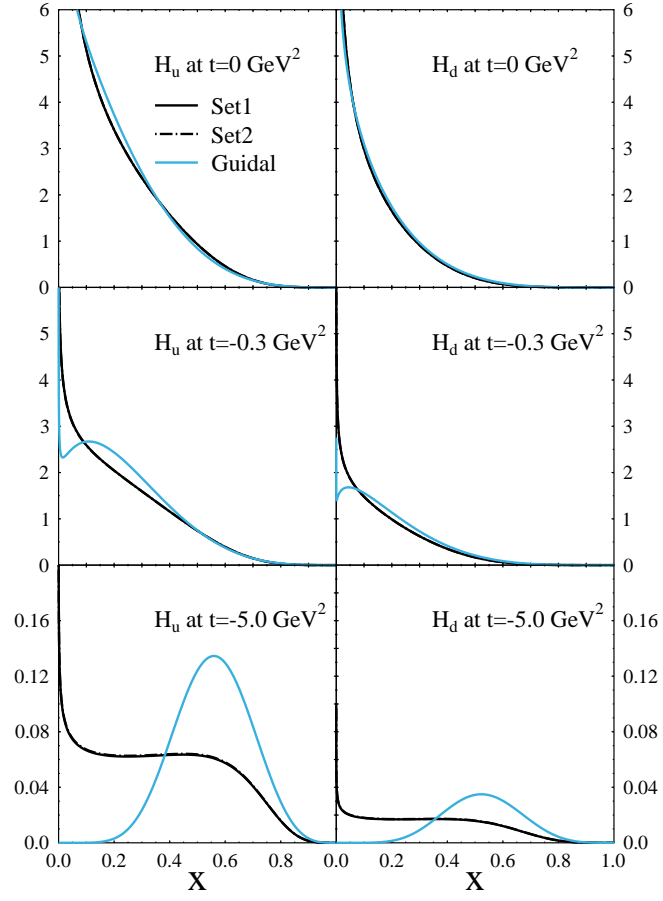


FIG. 14: (color online) Comparison with the quantitative extraction of GPDs from data from Ref. [14] at $Q^2 = 1$ GeV². Notations as in Fig. 13.

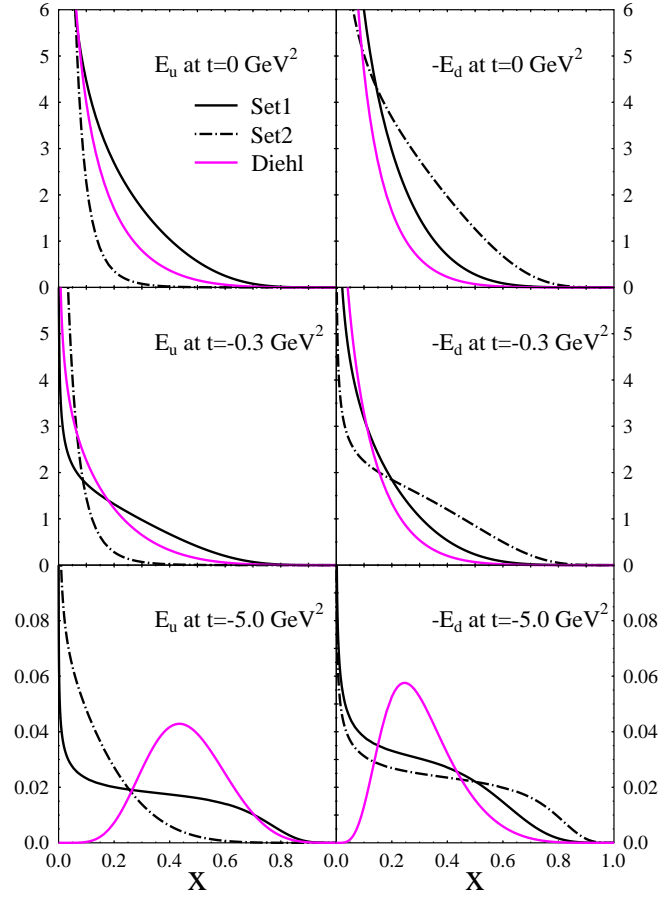


FIG. 15: (color online) Comparison with the quantitative extraction of GPDs from data from Ref. [13]. E_u (left) and $-E_d$ (right) as a function of X for $-t = 0, 0.3, 5 \text{ GeV}^2$, for our Parametrizations I and II, respectively evolved at $Q^2 = 4 \text{ GeV}^2$ used in Ref. [13].

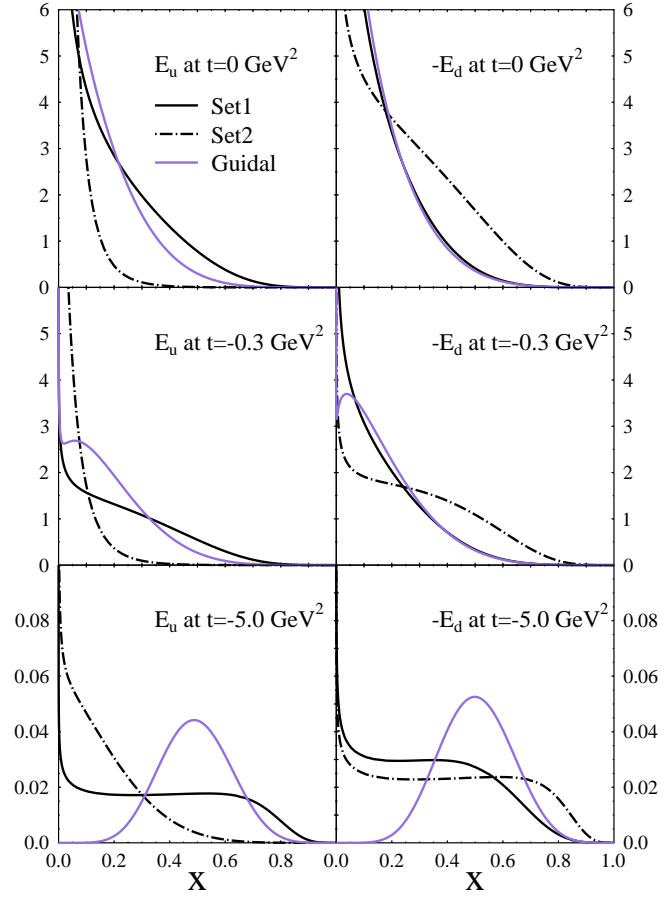


FIG. 16: (color online) Comparison with the quantitative extraction of GPDs from data from Ref. [14] at $Q^2 = 1$ GeV². Notations as in Fig. 15.

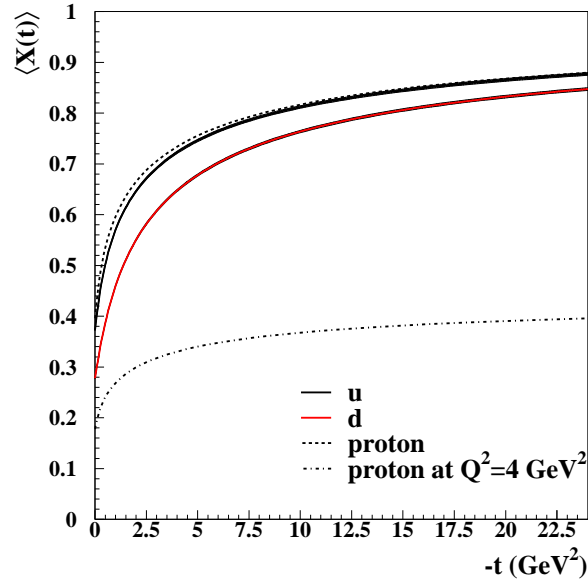


FIG. 17: (color online) Average value of X , Eq. (28, plotted vs. $-t$ at $Q^2 = Q_0^2$ for the u and d quarks contributions to the proton Dirac form factor, Eq. (11). The average value of X for the proton is also shown at $Q^2 = 4 \text{ GeV}^2$ (dot-dashed line).

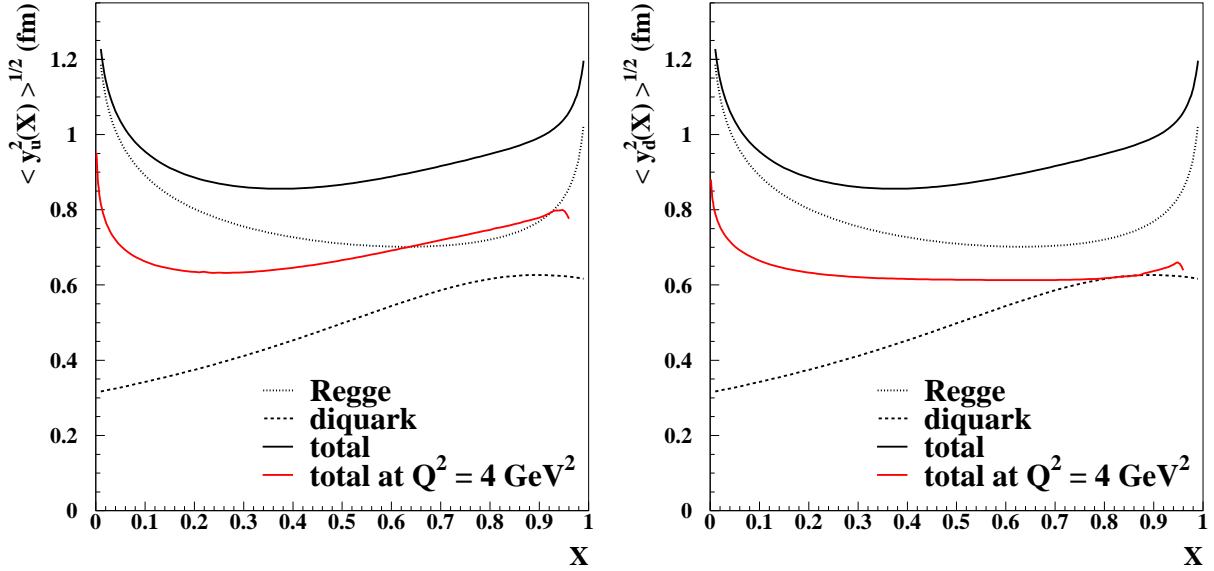


FIG. 18: (color online) $\langle y_u^2(X) \rangle$ (left panel) and $\langle y_d^2(X) \rangle$ (right panel) in our model, plotted vs. X . The contribution of the Regge and diquark term, respectively (see text) are shown separately along with the total result, at the initial scale. The total result is then evolved to $Q^2 = 4 \text{ GeV}^2$.

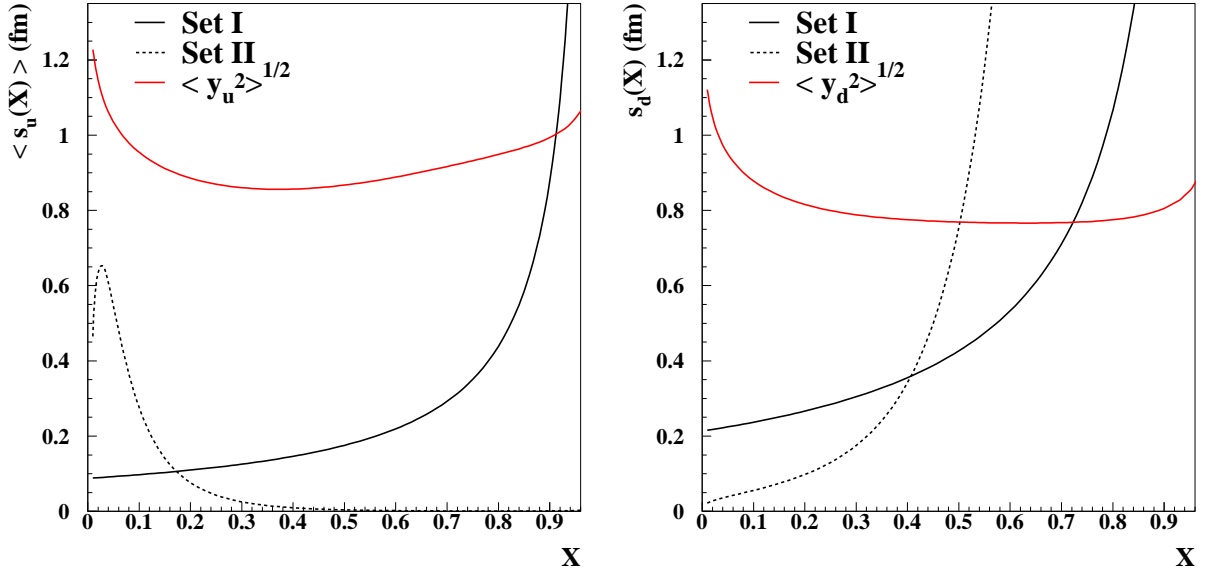


FIG. 19: (color online) $\langle s_u(X) \rangle$ (left panel) and $\langle s_d(X) \rangle$ (right panel) in our model, plotted vs. X . All curves are at the initial scale, Q_0^2 . The average interparton distance: $\langle y_q^2(X) \rangle^{1/2}$ is shown for comparison.

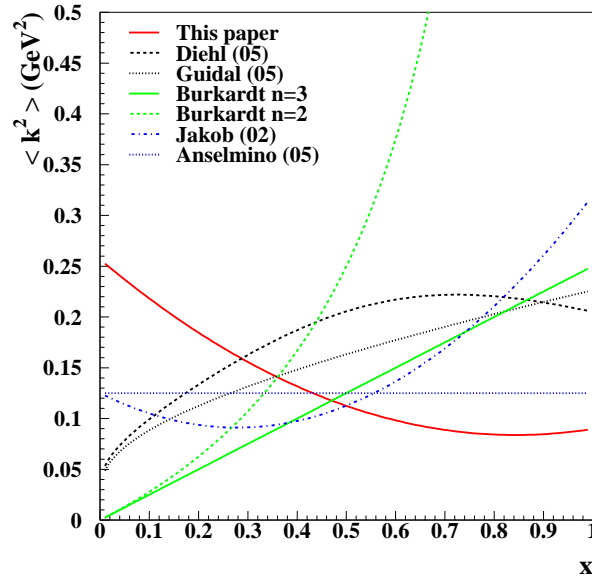


FIG. 20: (color online) The average intrinsic transverse momentum, Eq. (41b), compared to the value extracted from GPD parametrizations (Refs. [13], [14]); to the t -dependence conjecture of Ref. [55], and to models used in Semi-Inclusive DIS (SIDIS), Refs. [43] and [56].

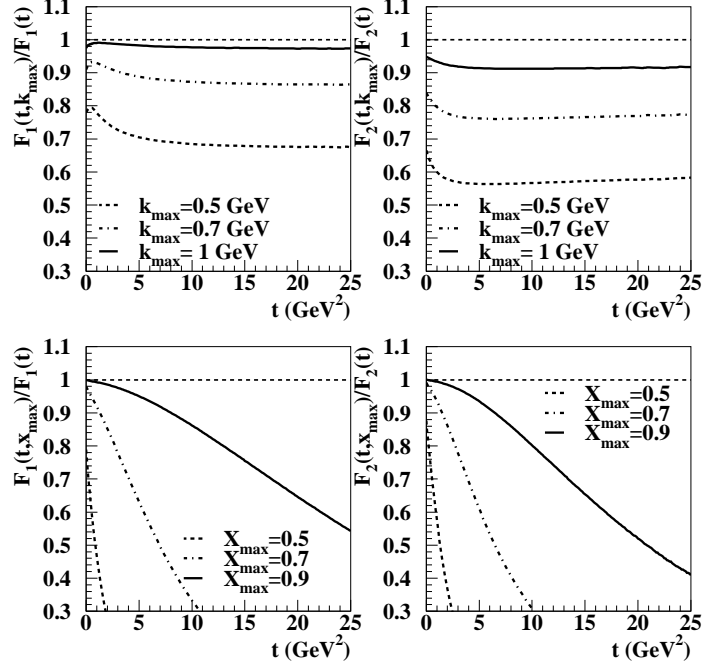


FIG. 21: Contribution of both the intrinsic transverse momentum components (upper panels) and X components (lower panels) to the proton form factors, $F_1^p(t)$ (left), and $F_2^p(t)$ (right).

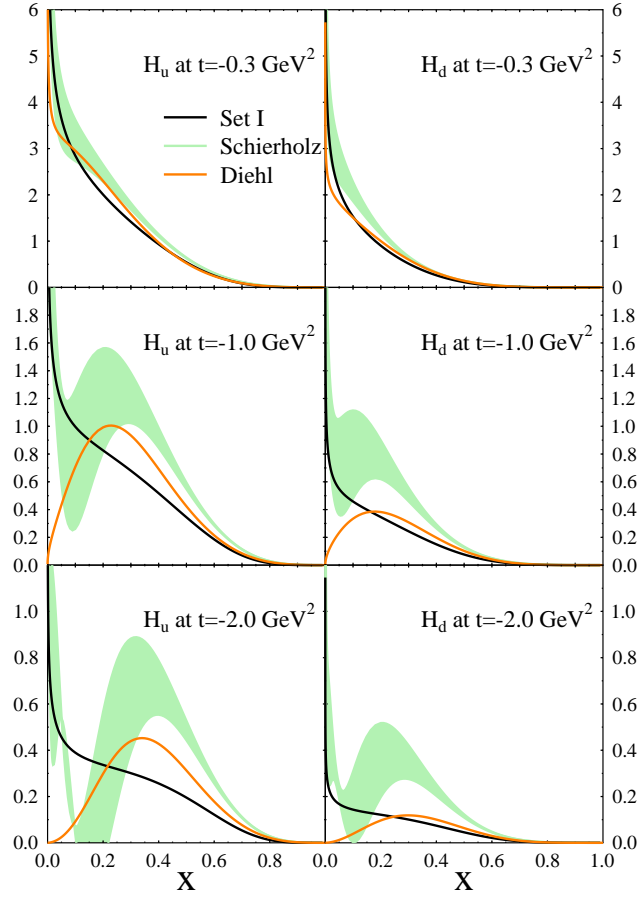


FIG. 22: (color online) Comparison of both the results of our analysis, and of Ref. [13], with an extraction of GPDs from lattice calculations according to the prescription of Ref. [36]. The band includes an estimate of the error from lattice calculations.

